Univerzita Karlova v Praze
Matematicko-fyzikální fakulta

DIPLOMOVÁ PRÁCE

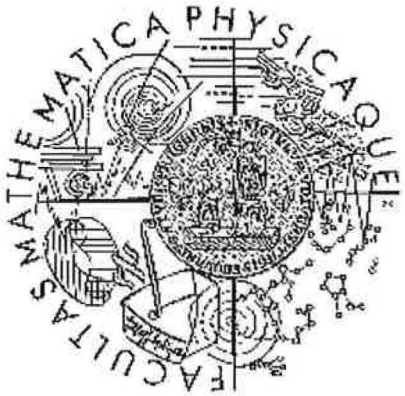

Pavel Kočica

Generace superkontinua v telekomunikačním pásmu 1550 nm s využitím mikrostrukturního optického vlákna

Fyzikální ústav UK

Vedoucí diplomové práce: Ing. Jiří Kaňka, CSc.,
Ústav radiotechniky a elektroniky AV ČR

Studijní program: Fyzika - Optika a optoelektronika,
studijní plán Optoelektronika a fotonika

Poděkování

Poděkovat bych chtěl zejména vedoucímu práce Ing. Jiří Kaňkovi, CSc. za jeho vzorné odborné vedení při studiu literatury, experimentální práci, numerických simulacích i zpracování výsledků. Dále bych chtěl poděkovat i dalším pracovníkům Oddělení vlnovodné fotoniky Ústavu radiotechniky a elektroniky AV ČR, jmenovitě konzultantovi Dr. Ing. Pavlu Honzátkovi za jeho cenné rady a připomínky a Ing. Miroslavu Karáskovi, DrSc. za poskytnuté experimentální vybavení.

Prohlašuji, že jsem svou diplomovou práci napsal samostatně a výhradně s použitím citovaných pramenů. Souhlasím se zapůjčováním práce.

V Praze dne 07.04.2006 Pavel Kočica

Contents

Název práce : Generace superkontinua v telekomunikačním pásmu 1550 nm s využitím mikrostrukturního optického vlákna
Autor: Pavel Kočica
Katedra (ústav): Fyzikální ústav UK
Vedoucí diplomové práce: Ing. Jiří Kaňka, CSc., Ústav radiotechniky a elektroniky AV ČR
e-mail vedoucího: kanka@ure.cas.cz
Abstrakt: Tato diplomová práce přináší experimentální a numerické demonstrace generace superkontinua v mikrostrukturním optickém vlákně použitím optických pulsů generovaných vláknovými lasery. Je podán přehled současného stavu výzkumu v generaci superkontinua. V teoretické části jsou popsány hlavní procesy, které mají vliv na puls šířící se v optickém vlákně. Jsou prezentovány moderní přístupy používané při generaci superkontinua (např. použití vláknových laserů, similaritonů a mikrostrukturních optických vláken). Jsou vysvětleny principy optických konumikací se zaměřením na aplikace superkontinua. Experimentálně jsou demonstrovány možnosti aplikací superkontinua v optických komunikacích v oblasti 1550 – 1560 nm. Vysoce nelineární konvenční optická vlákna jsou použita pro srovnání vlastností superkontinua generovaného v mikrostrukturním vláknu a v delších konvenčních vláknech. Spektrální šířka a vyrovnanost generovaného superkontinua jsou optimalizovány pomocí nastavení parametrů vstupních pulsů (šířka, centrální vlnová délka, špičkový výkon). Je upozorněno na experimentální problémy při generaci superkontinua (zesilování ultrakrátkých pulsů, vlivy spekter laseru a zesilovače atd.) a jsou prezentovány cesty k jejich řešení.
Klíčová slova: superkontinuum, optické solitony, mikrostrukturní optická vlákna, vláknové lasery, optické komunikace

Title: Supercontinuum generation in telecommunication range 1550 nm using a microstructured optical fibre
Author: Pavel Kočica
Department: Institute of Physics of Charles University
Supervisor: Ing. Jiří Kaňka, CSc., Institute of Radio Engineering and Electronics of Czech Academy of Sciences
Supervisor's e-mail address: kanka@ure.cas.cz
Abstract: This master thesis brings both experimental and numerical demonstrations of the supercontinuum generation in a microstructured optical fibre using optical pulses generated in fibre lasers. An overview of present situation in the research of supercontinuum generation is given. In theoretical part, main processes affecting the pulse propagation in optical fibres are described. Modern approaches used in the supercontinuum generation are presented, for example using fibre lasers, similaritons and microstructured optical fibres). Principles of optical communications are explained with respect to applications of a supercontinuum. Possibilities of supercontinuum applications in optical communications are experimentally demonstrated in the range 1550 – 1560 nm. Highly-nonlinear conventional optical fibres are used to compare the properties of the supercontinuum generated in the microstructured optical fibre and in longer conventional fibres. The spectral bandwidth and flatness of the generated supercontinuum are optimized by adjusting the parameters of input pulses (width, central wavelength, peak power). Experimental problems of the supercontinuum generation (amplification of ultrashort pulses, influences of laser and amplifier spectra etc.) are pointed out and ways to their solution are presented.
Keywords: supercontinuum, optical solitons, microstructured optical fibres, fibre lasers, optical communications

1. Introduction

Nonlinear processes in optical fibres can lead to a spectral broadening of a propagating optical pulse. This phenomenon was discovered in 1970. In last few years (let us say since 2000) a great focus in research is imposed to using highly nonlinear fibres for generating a ultra-broadband spectrum (extended over more than 1000 nm in some experiments), usually called supercontinuum (SC). Main processes leading to the generation of SC in optical fibres are self-phase modulation, four-wave mixing (when the phase-matching condition is satisfied) and Raman scattering (expecially in long fibres).

A SC source is a new type of a light source that combines features needed in applications: a high output power, a broad and flat spectrum, a high degree of spatial coherence. In applications, SC sources can significantly improve a signal-to-noise ratio, reduce measurement time and widen the spectral range for measurements. Many companies produce SC sources commercially (see [1]).

A supercontinuum generated in the visible regime has lots of applications. In a photonic-device testing, SC is used for measuring the optical properties of waveguides and fibres at various wavelengths (measurements of attenuation, testing lasers and amplifiers, characterising polymer waveguides). Low-coherence "white light" interferometry uses SC for a determination of defects positions in waveguides. In the spectroscopy, a high degree of spatial coherence of SC allows the radiation to be collimated to a narrow beam for measuring small samples in biology, chemistry, medicine, physics and environmental monitoring. The optical coherence tomography is a medical application, where SC sources allow to improve spatial resolution and to speed up a scan due to a high repetition rate.

Recently, a lot of applications were found in optical telecommunications that require a SC source operating in the 1550-nm telecommunication window. One of these applications is, for instance, a realisation of a tunable optical clock translator for high-speed optical time division multiplexing (OTDM). The optical clock signal is transmitted simultaneously with the time-multiplexed data and it is used for their demultiplexing in the receiver (see [2], [3]). Another perspective usage of SC sources in telecommunication area is wavelength division multiplexing (WDM) source. In WDM systems, a signal is transmitted synchronously in many spectral channels. Flat and broadband SC (generated using an actively mode-locked laser) combined with a spectral filter can be used as a source for the spectral channels. A signal-to-noise ratio is improved due to high coherence of SC. A WDM system with SC as a source has been already commercially realized.

Principal parts of the SC source are a pulsed laser, a fibre amplifier and a nonlinear element, in which nonlinear effects lead to the spectral broadening. A realization of an all-fibre SC source without bulk optics is required, because fibres can be fusion spliced to each other with the minimal loss and with simplifying an experimental arrangement. Fibre lasers are mostly used as sources of ultrashort pulses required for SC generation. They can produce sub-picosecond pulses with a high peak power and a high repetition rate [4]. The pulses are amplified to further increase their peak power, usually in erbium-doped fibre amplifiers. As a realization of the nonlinear element, highly nonlinear, single-mode silica optical fibres are used. A microstructured optical fibre (MOF) is a new type of an optical fibre which enables much better nonlinear and dispersive characteristics than standard fibres.

The tunable optical clock translator for OTDM communication systems can be realized by a spectral slicing of the generated SC using a tunable filter. When an autocorrelation trace is detectable in the selected spectral part of SC, it proves that the clock signal at the pump wavelength is converted to another wavelength. This converted signal can be used as a synchronization signal in OTDM systems. A WDM source can be demostrated

experimentally using a multiplexor, which divides the spectrum into many spectral channels.
The main subject of this master thesis is optimizing SC characteristics (bandwidth, flatness, coherence) using available experimental equipment. The characteristics of SC are optimized with respect to applications of SC in OTDM and WDM communication systems. Both experiments and simulations were used for this purpose. The experiments were realized at Guided-wave Photonics Department of Institute of Radio Engineering and Electronics of Czech Academy of Sciences. A computer program based on the split-step Fourier method was developed in order to simulate the pulse propagation in nonlinear fibres. Further, the thesis gives an overview of modern methods used in SC generation (fibre lasers, similaritons and microstructured optical fibres) and in telecommunication applications (OTDM and WDM systems).
Chapter 2 focuses on microstructured optical fibres, which are widely used in SC generation. Chapter 3 reports a present research situation in the SC generation and related branches (fibre lasers, amplifiers, compressors). Chapter 4 provides theoretical fundamentals of the thesis. Physical effects affecting a pulse during its propagation in an optical fibre are described. Theoretical fundamentals of fibre lasers as well as basic principles of optical communication systems are discussed, too. Results of our experiments and simulations are presented in Chapter 5. Chapter 6 brings a conclusion carried out from experiments and numerical simulations. The numerical approach to the solution of the propagation equation in the optical fibre is presented in Appendix A

2. Microstructured optical fibres

Propagation of light in conventional silica optical fibres is based on the difference between the refractive indices of the core (n_1) and the cladding (n_2). In step-index fibres, refractive indices n_1 and n_2 are independent of distance from fibre axis. These fibres operate on a principle of the total internal reflection on the boundary between the core and the cladding. In graded-index fibres, the refractive index of the core descends from fibre axis to the core-cladding boundary. Therefore, light beams propagate in incurvate trajectories. Further, let us assume step-index fibres.
Light can propagate in optical fibre in guided modes. In optical communications, single-mode fibres are mostly used, because of limiting factors of modal dispersion in multi-mode fibres. Condition for the single-mode regime of the fibre (derived in [5]) is

$$V = 2\pi \frac{a}{\lambda_0} \text{N.A.} < 2.405 , \tag{2.1}$$

where a is the core radius, λ_0 is a wavelength of the propagation light and N.A. stands for the numerical aperture:

$$\text{N.A.} = \sqrt{n_1^2 - n_2^2} . \tag{2.2}$$

Parameter V is called the normed frequency or V-parameter of the optical fibre [5].
A microstructured optical fibre (MOF) is a new type of optical fibres. MOFs can be divided into two categories according to a propagation principle: a solid-core MOF (an index-guided MOF) and a hollow-core MOF (a photonic bandgap MOF).

In the solid-core MOF light is guided due to the total internal reflection similarly to conventional step-index fibres. The required index difference between the core and the cladding is created by presence of air holes in the cladding, so the average refractive index of the cladding is lower than the refractive index of the core. The advantage of this type of MOF is that optical properties such as a mode shape, nonlinearity, group-velocity dispersion (GVD) and birefringence can be varied over a wide range by varying the arrangement of holes. The effective difference between refractive indices of the cladding and the core descends with increasing the wavelength, because longer wavelengths differentiate the microstructure in the cladding less than shorter wavelengths. The effective area of an optical field can be very small due to a high optical contrast. Fig. 2.1 shows an example of a solid-core MOF.

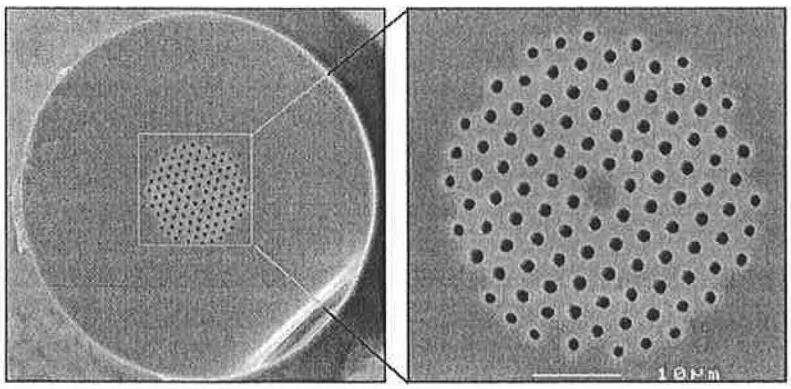

Fig. 2.1 Scanning Electron Micrograph of the solid-core fibre cross section. Holes have a hexagonal symmetry (after [1]).

Other mechanism is employed in a hollow core MOF: due to a periodic arrangement of the holes in the cladding, the photonic bandgap effect is created, so the cladding works as an ideal mirror for the light travelling through the fibre. However, this effect appears only for certain bands of photon energies (or wavelenghts). The core is filled only with air (see Fig. 2.2) – this results in extremely low optical nonlinearity. Photonic bandgap MOFs can be used for pulse compression [6].

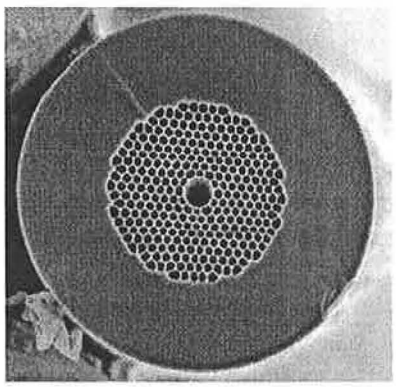

Fig. 2.2 Cross section of the hollow-core MOF. Light is guided in the hollow core due to a periodic structure of the holes in the cladding (after [1]).

In our experiments we used the microstructured optical fibre NL-1550-NEG-1 [7] fabricated by Crystal Fibre A/S (www.crystal-fibre.com). It is the index-guided silica fibre with small positive dispersion. Parameters of NL-1550-NEG-1 are given in Tab. 2.1.

Tab. 2.1 Parameters of NL-1550-NEG-1 (after [7]).

Length	10 m
Average core diameter	2.1 ± 0.3 μm
Dispersion parameter D in 1510-1620 nm	> -1.7 ps/nm/km
Attenuation constant α in 1510-1620 nm	< 9 dB/km
Mode field diameter at 1550 nm	2.8 ± 0.5 μm
Numerical aperture at 1550 nm	0.40 ± 0.05
Nonlinear coefficient γ at 1550 nm	~11 $(Wkm)^{-1}$

A cross section of the fibre and the spectral dependence of its dispersion parameter D are shown in Fig. 2.3.

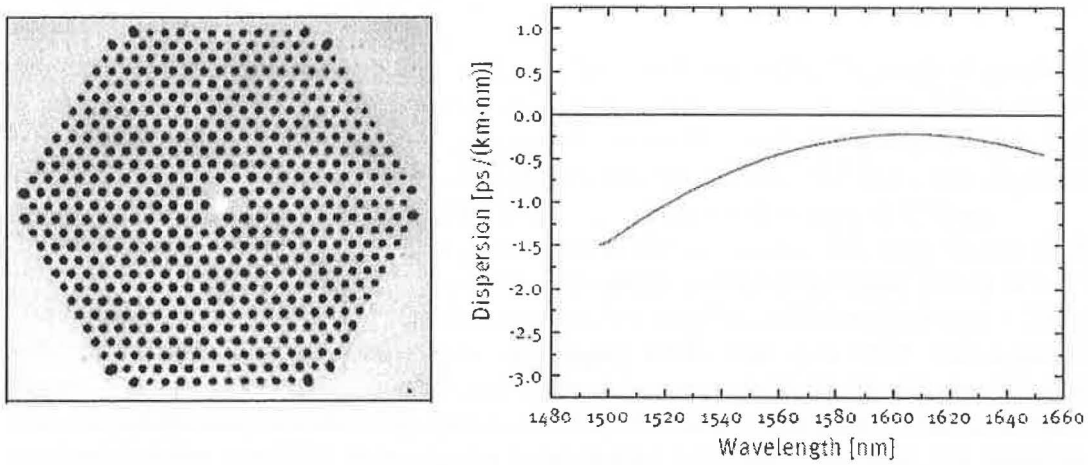

(a) (b)

Fig. 2.3 (a) Cross section of NL-1550-NEG-1; (b) dependence of the dispersion parameter D of NL-1550-NEG-1 on wavelength (after [7]).

Negative values of D in Fig. 2.3b indicate positive group velocity dispersion (definition of this parameter is in Sec. 4.3.3).

3. Overview of present situation in SC generation and related branches

3.1 Recent experiments demonstrating SC generation at 1550 nm

In one experiment [2], a pulse train was generated by a mode-locked fibre ring laser at 1550.5 nm with a repetition rate of 10 GHz, amplified by an erbium-doped fibre amplifier, compressed in a nonlinear pulse compressor and then coupled into a 50-m long highly-

nonlinear MOF with a zero-dispersion wavelength of 1552 nm, the nonlinear coefficient 18 $W^{-1}\cdot km^{-1}$ and birefringence 1.1×10^{-4}. The MOF was spliced to standard single-mode fibre pigtails, so this device is entirely compatible with the fibre optics technology. The pulse FWHM was in the range from 0.3 to 2.5 ps. The generated SC extends over 60 nm and 75 nm for light launched parallel to the principal polarization axes of the fibre. The application for optical time-division multiplexing (OTDM) systems was realized by the spectral filtering of the SC. The converted clock signals at 1578.4 nm and 1574.1 nm were obtained from the SC.

A paper [8] reports the fabrication and properties of a soft glass MOF with zero or anomalous GVD at wavelengths around 1550 nm. The generation of an ultrabroadband SC using 1550 nm ultrafast pump source was also demonstrated. Main technology focus was intended to optimize GVD while maintaining high nonlinearity. Dispersion at 1550 nm was around -30 $ps\cdot nm^{-1}\cdot km^{-1}$, towards shorter wavelengths it rapidly became more negative. The zero-dispersion wavelength could be moved by changing the core diameter. The SC generation experiment was performed using an ultrashort optical parametric oscillator with 100-fs pulse duration at 1550 nm. The pulse repetition was 80 MHz and the average output power of the laser was 200 mW. The generated SC broadened from 350 nm to 2200 nm. Such fibres with a mode locked fibre laser source at 1550 nm will enable the generation of the large-spanning SC to make a compact and stable high-brightness broadband light source.

Another MOF suitable for the SC generation is introduced in [9]. The optical properties were designed by varying the diameter of air-holes along the fibre radius. This type of a hole arrangement provided an easy concurrent control of dispersion, the dispersion slope and nonlinearity. The fibre had a nonlinear coefficient of 34.5 $W^{-1}\cdot km^{-1}$, the dispersion coefficient of -0.12 $ps\cdot km^{-1}\cdot nm^{-1}$ and the dispersion slope equal to zero at 1550 nm.

In a paper [10] there is reported a generation of the symmetric SC over 40 nm in the 1550 nm region using 1562-nm, 2.2-ps, 40-GHz optical pulses with a peak power of 6.3 W. The pulses were amplified in an erbium-doped fibre amplifier and launched into a 200 m-long, dispersion-flattened polarization-maintaining MOF. The used MOF had a specific design. Four air holes in the central part of the fibre provided high birefringence, which realized polarization-maintaining operation. The fibre had a silica core with an elliptical Ge-doped centre core (for reducing the confinement loss and controlling the dispersion characteristics). The low dispersion slope was realised. Dispersion and the dispersion slope at 1550 nm were -0.23 $ps\cdot km^{-1}\cdot nm^{-1}$ and 0.01 $ps\cdot km^{-1}\cdot nm^{-2}$, respectively. Modal birefringence at 1550 nm was 1.3×10^{-3}, nonlinear parameter γ was 19 $W^{-1}km^{-1}$. Such a fibre can be used as a part of a multi-channel optical source for WDM communication and photonic network systems.

A paper [11] brings the description of the SC generation in a highly-nonlinear bismuth-oxide fibre. The nonlinear coefficient of the fibre was extremely high, 1100 $W^{-1}\cdot km^{-1}$. Normal dispersion was also high, -250 $ps\cdot km^{-1}\cdot nm^{-1}$. The generated SC was smooth and unstructured. The SC spanning from 1200 nm to 1800 nm was generated in a 2-cm piece of the fibre by the pulse source with the average input power 32 mW. As a result of the spectral broadening, the pulse width was compressed from 150 fs to 25 fs.

A paper [12] reports the differences in SC-generation mechanisms, when the nonlinear fibre is pumped in the normal- and anomalous-dispersion regime. In the anomalous-dispersion regime, a spectral broadening is caused by decay of the initial *N*th-order soliton into *N* fundamental solitons (see Sec. 4.5) due to the influence of higher-order dispersion and Raman scattering. In the normal-dispersion regime, self-phase modulation initiates the SC generation, further spectral broadening is provided by the combination of four-wave mixing and Raman processes.

In another experiment [13], the effect of the initial chirp to the SC bandwidth was examined. It was pointed out that there exists an optimal chirp, which maximizes the bandwidth of the generated SC. The SC bandwidth is related to the time evolution of the propagating pulse (splitting into more long-wavelength solitons in the anomalous-dispersion regime, which shed the dispersive waves.). In the anomalous-dispersion regime, the positive initial chirp improved the SC generation while the opposite occurred for the negative initial chirp.

3.2 Applications of SC generated in the telecommunication range

In an experiment [14] a SC source was used for the multiple optical carrier generation. This was needed for one of the largest commercial systems, a 10-Gbit/s, 160-channel WDM system. In WDM networks it is expected the number of transmission wavelengths ranging from 100 to 1000. A SC source is a promising method for multiple carrier source. The optical carriers could be obtained by a spectral slicing of the SC spectrum. Multicarriers from the SC source were produced with the mode-locked laser diode (generating 4.3-ps, 12.5-GHz pulse train) and the polarization-maintaining dispersion-flattened fibre. SC generated around 1560 nm exhibited greater than 100-nm spectral broadening (more than 1000 channels). Long-term stability of the absolute frequency of one channel was better than 0.3 GHz, much smaller than channel spacing. A signal-to-noise ratio was sufficient for using in WDM systems. By optimization of the design of the SC fibre and the pumping condition there can be developed WDM networks with high bit rates (40 Gbit/s) and long transmission distances (> 1000 km).
In a paper [15] the characterization of high-index contrast photonic circuits is reported. The ultra-broadband SC covering range 1200 nm – 2000 nm was generated by pulses with a central wavelength of 1550 nm. The generated SC was used for rapid and high-resolution measurements of nano-scale photonic crystal microcavities. The ultra-broadband SC brings a great simplification to such measurements, because it substitutes the tunable lasers, which are not readily available at this spectral range. The high resolution 0.1 nm was reached when measuring the microcavity modal frequencies, quality factors and the photonic bandgap wavelengths.
In another experiment [16], a SC broadening from 400 nm to 1750 nm generated with pulses at 1550 nm was used for the formation of the optical waveguides in the silica glass. It is pointed out that SC generated at 1550 nm improves the waveguide parameters and the energy limitations unlike the SC generated at 800 nm.

3.3 Progress in amplification of sub-picosecond pulses

Nonlinearity in the amplifier can have detrimental influence on the propagating ultrashort pulse and can lead even to decay of the pulse. Therefore, the pulse width must be increased to several picoseconds before amplification. This broadening leads to decreasing the peak power of the pulse and to suppressing the nonlinear effects in the amplifier. After amplification, the pulses can be compressed again to achieve a high peak power before they are launched into the nonlinear element for the SC generation. Recently, a new propagation regime in the amplifier was introduced: in a combination of normal dispersion, nonlinearity and a distributed gain in the amplifier, the propagating pulse can acquire a parabolic shape and a high linear chirp. The pulse propagates self-similarly in the amplifier, maintaining its parabolic shape. These parabolic pulses are called similaritons. Due to their

high linear chirp, similaritons can be efficiently compressed after an amplification using a grating compressor or an anomalous-dispersion fibre. Similaritons are under intensive study, because they are suitable for applications, where a high amplification of pulses is required.
In one experiment [17], the self-similar parabolic pulses (similaritons) were generated in a Raman amplifier consisting of a standard 5.3-km long non-zero dispersion-shifted fibre using watt-level continuous-wave pump source at 1455 nm combined with input signal pulses at 1550 nm. The fibre has the nonlinear coefficient 2.23 $W^{-1}\cdot km^{-1}$, second-order dispersion was 4.89 $ps^2\cdot km^{-1}$ and third-order dispersion was 0.109 $ps^3\cdot km^{-1}$. An intensity and chirp of the output pulses were measured with frequency resolved optical gating. The linear chirp across the whole pulse width was observed.
In another experiment [18], there was introduced a pulse synthesis method using similaritons, generated in a standard 7.3-km long non-zero dispersion-shifted fibre. Parameters of the used fibre at a wavelength of 1500 nm were: the nonlinear coefficient 2.0 $W^{-1}\cdot km^{-1}$, dispersion of 2.0 $ps^2\cdot km^{-1}$, the dispersion slope 0.081 $ps\cdot nm^{-1}\cdot km^{-1}$ and the Raman-amplification gain 2.38 $dB\cdot km^{-1}$. Synthesized pulses were independent of the intensity and chirp profiles, peak power and wavelength of the original input pulse.

4. Theoretical fundamentals of SC generation

4.1 Supercontinuum source, quality of supercontinuum

Principal parts of the SC source are a pulse source (a fibre laser), an amplifier and a nonlinear fibre. All of these parts should be realized by the optical fibres in order to minimize the need of bulk optics. The ultrashort-pulse fibre lasers generate a train of pulses, which are further transformed in other parts of the experimental setup. The pulse-to-pulse energy stability is required. The amplification of the pulses from the laser output is usually realized by the fibre amplifiers doped by rare earths (Yb, Er). Then the pulses are launched into the nonlinear fibre, where the nonlinear effects (self-phase modulation, four-wave mixing, Raman scattering) lead to the spectral broadening to obtain SC.
The quality of the SC at 1550 nm generated in the nonlinear fibre is characterized with respect to its applications in optical telecommunications. The main characteristics of SC are flatness, bandwidth and uniformity of coherence across the spectrum. These characteristics are influenced by the parameters of the input pulse (peak power, width, initial chirp and polarization) and of the nonlinear fibre (mainly nonlinear and dispersion characteristics). Latest experiments show that the quality of SC is better when generating in the normal-dispersion regime of the nonlinear fibre, where the pulse is not affected by the detrimental features of the soliton propagation.
Following sections bring the theoretical fundamentals of the pulse propagation in optical fibres. Sec. 4.2 focuses on the derivation of the nonlinear Schrödinger equation, which describes the propagation of the slowly-varying envelope of the pulse. The main physical mechanism affecting the propagating pulse is the interplay of its initial chirp with the chirps caused by dispersive and nonlinear effects. These effects are described in Secs. 4.3 and 4.4, respectively. Soliton regime of the pulse propagation is theoretically characterized in Sec. 4.5. Sec. 4.6 provides theoretical fundamentals of fibre lasers. Concepts of OTDM and WDM communication systems are introduced in Sec. 4.7.

4.2 Propagation equation

This section brings a derivation of the nonlinear Schrödinger equation for the slowly-varying envelope of the optical pulse. It is a fundamental equation describing the propagation of optical pulse in the fibre [19].
The evolution of an optical field in optical fibres is described by Maxwell's equations:

$$\nabla \times \mathbf{E}(\mathbf{r},t) = -\frac{\partial \mathbf{B}(\mathbf{r},t)}{\partial t}, \tag{4.2.1}$$

$$\nabla \times \mathbf{H}(\mathbf{r},t) = \boldsymbol{j}_f(\mathbf{r},t) + \frac{\partial \mathbf{D}(\mathbf{r},t)}{\partial t}, \tag{4.2.2}$$

$$\nabla \cdot \mathbf{D}(\mathbf{r},t) = \rho_f(\mathbf{r},t), \tag{4.2.3}$$

$$\nabla \cdot \mathbf{B}(\mathbf{r},t) = 0, \tag{4.2.4}$$

where $\mathbf{E}(\mathbf{r},t)$ and $\mathbf{H}(\mathbf{r},t)$ are electric and magnetic field vectors, $\mathbf{D}(\mathbf{r},t)$ and $\mathbf{B}(\mathbf{r},t)$ are electric and magnetic flux densities, respectively. Sources of the electromagnetic field represented by the current density vector $\mathbf{j}_f(\mathbf{r},t)$ and the charge density ρ_f are not considered in optical fibres, therefore $\mathbf{j}_f(\mathbf{r},t) = \mathbf{0}$ and $\rho_f(\mathbf{r},t) = 0$.
The equations above must be supplemented with material equations:

$$\mathbf{D}(\mathbf{r},t) = \varepsilon_0 \mathbf{E}(\mathbf{r},t) + \mathbf{P}(\mathbf{r},t), \tag{4.2.5}$$

$$\mathbf{B}(\mathbf{r},t) = \mu_0 \mathbf{H}(\mathbf{r},t) + \mathbf{M}(\mathbf{r},t), \tag{4.2.6}$$

where $\mathbf{P}(\mathbf{r},t)$ and $\mathbf{M}(\mathbf{r},t)$ are the electric and magnetic polarizations, ε_0 and μ_0 the vacuum permittivity and permeability, respectively. An optical fibre is a nonmagnetic medium, where $\mathbf{M}(\mathbf{r},t) = \mathbf{0}$.
Using standard steps, the wave equation can be derived in the form

$$\nabla^2 \mathbf{E}(\mathbf{r},t) - \frac{1}{c^2}\frac{\partial^2 \mathbf{E}(\mathbf{r},t)}{\partial t^2} = \mu_0 \frac{\partial^2 \mathbf{P}_L(\mathbf{r},t)}{\partial t^2} + \mu_0 \frac{\partial^2 \mathbf{P}_{NL}(\mathbf{r},t)}{\partial t^2}, \tag{4.2.7}$$

where c is the light velocity in the vacuum and we introduced the linear $\mathbf{P}_L(\mathbf{r},t)$ and nonlinear $\mathbf{P}_{NL}(\mathbf{r},t)$ part of the electric polarization $\mathbf{P}(\mathbf{r},t)$ by the relation

$$\mathbf{P}(\mathbf{r},t) = \mathbf{P}_L(\mathbf{r},t) + \mathbf{P}_{NL}(\mathbf{r},t). \tag{4.2.8}$$

These parts of the electric polarization are coupled with electric field by the equations

$$\mathbf{P}_L(\mathbf{r},t) = \varepsilon_0 \int_{-\infty}^{\infty} \chi^{(1)}(t-t_1)\mathbf{E}(\mathbf{r},t_1)dt_1, \tag{4.2.9}$$

$$\mathbf{P}_{NL}(\mathbf{r},t) = \varepsilon_0 \int_{-\infty}^{\infty}\int_{-\infty}^{\infty}\int_{-\infty}^{\infty} \chi^{(3)}(t-t_1,t-t_2,t-t_3)\mathbf{E}(\mathbf{r},t_1)\mathbf{E}(\mathbf{r},t_2)\mathbf{E}(\mathbf{r},t_3)dt_1dt_2dt_3, \tag{4.2.10}$$

where $\chi^{(1)}$ is the first-order electric susceptibility and $\chi^{(3)}$ is the third-order electric susceptibility. The second-order susceptibility $\chi^{(2)}$ vanishes in materials with an inverse symmetry such as SiO_2.

Derivation of the propagation equation from (4.2.7) requires making several simplifications. First, we will use a slowly-varying-envelope approximation, which enables to separate the rapidly varying part of the optical field and the envelope function of the optical field, which varies slowly at the scale of optical period. Second, the spectral width of the pulse $\Delta\omega$ is assumed to satisfy the condition $\Delta\omega/\omega_0 \ll 1$. This is valid for pulse widths ≥ 0.1 ps. Third, the optical field is expected to maintain its polarization state during the propagation along the fibre length. Violation of this assumption would require a pair of coupled propagation equations for each polarization component, as described in [19]. Fourth, $\mathbf{P}_{NL}$ is treated as a small perturbation to $\mathbf{P}_L$. This assumption is satisfied in optical fibres. Fifth, the nonlinear response of the medium is assumed to be instantaneous, which allows to simplify (4.2.10) to the form

$$\mathbf{P}_{NL}(\mathbf{r},t) = \varepsilon_0 \chi^{(3)} \mathbf{E}(\mathrm{r},t)\mathbf{E}(\mathrm{r},t)\mathbf{E}(\mathrm{r},t)\,. \tag{4.2.11}$$

Following the slowly-varying-envelope approximation, let us write the electric field in the form

$$\mathbf{E}(\mathbf{r},t) = \frac{1}{2}\hat{x}[\overline{E}(\mathbf{r},t)\exp(-i\omega_0 t) + \mathrm{c.c.}]\,, \tag{4.2.12}$$

$$\mathbf{P}_L(\mathbf{r},t) = \frac{1}{2}\hat{x}[\overline{P}_L(\mathbf{r},t)\exp(-i\omega_0 t) + \mathrm{c.c.}]\,, \tag{4.2.13}$$

$$\mathbf{P}_{NL}(\mathbf{r},t) = \frac{1}{2}\hat{x}[\overline{P}_{NL}(\mathbf{r},t)\exp(-i\omega_0 t) + \mathrm{c.c.}]\,, \tag{4.2.14}$$

where $\hat{x}$ is the polarization unit vector (the electric field is assumed to be linearly polarized along the x axis), ω_0 is the central frequency of the wave, $\overline{E}(\mathbf{r},t)$, $\overline{P}_L(\mathbf{r},t)$ and $\overline{P}_{NL}(\mathbf{r},t)$ are slowly-varying functions of time and c.c. means complex conjugate.
The Fourier transform $\tilde{E}(\mathbf{r},\omega-\omega_0)$ of $\overline{E}(\mathbf{r},t)$ is given by

$$\tilde{E}(\mathbf{r},\omega-\omega_0) = \int_{-\infty}^{\infty} \overline{E}(\mathbf{r},t)\exp[i(\omega-\omega_0)t]dt\,. \tag{4.2.15}$$

Taking the Fourier transform of (4.2.7) and following the approximations above, the wave equation can be written in the form

$$\nabla^2\tilde{E} + \varepsilon(\omega)k_0^2\tilde{E} = 0\,, \tag{4.2.16}$$

where $k_0 = \omega_0/c$ and $\varepsilon(\omega)$ is the dielectric constant given by

$$\varepsilon(\omega) = 1 + \tilde{\chi}^{(1)}_{xx}(\omega) + \frac{3}{4}\tilde{\chi}^{(3)}_{xxxx}\left|\overline{E}(\mathbf{r},t)\right|^2\,. \tag{4.2.17}$$

We assume the solution of (4.2.16) in the form

$$\tilde{E}(\mathbf{r},\omega-\omega_0) = F(x,y)\tilde{A}(z,\omega-\omega_0)\exp(i\beta_0 z)\,, \tag{4.2.18}$$

where $F(x,y)$ is the transverse field distribution, β_0 is the wavenumber and $\tilde{A}(z,\omega-\omega_0)$ is a slowly varying function of z. In the case of a single-mode fibre, $F(x,y)$ is the modal distribution of the fundamental fibre mode HE_{11}, which is usually approximated by the Gaussian function.
By substituting (4.2.18) to (4.2.16) and using a slowly-varying-envelope approximation, we obtain the equation for $\tilde{A}$:

$$2i\beta_0\frac{\partial\tilde{A}}{\partial z}+(\bar{\beta}^2-\beta_0^2)\tilde{A}=0, \tag{4.2.19}$$

where $\bar{\beta}$ can be obtained by solving an eigenvalue equation for the modal distribution $F(x,y)$ using the first-order perturbation theory. The corresponding eigenvalue $\bar{\beta}$ is given by

$$\bar{\beta}(\omega)=\beta(\omega)+\Delta\beta, \tag{4.2.20}$$

where $\Delta\beta$ is the correction in the first order of the perturbation theory. It includes the effect of fibre loss and nonlinearity. The unperturbed propagation constant $\beta(\omega)$ can be expanded (following approximation of small spectral widths) into a Taylor series about the carrier frequency:

$$\beta(\omega)=\beta_0+(\omega-\omega_0)\beta_1+\frac{1}{2}(\omega-\omega_0)^2\beta_2+\frac{1}{6}(\omega-\omega_0)^3\beta_3+\ldots \tag{4.2.21}$$

where

$$\beta_n=\left(\frac{d^n\beta}{d\omega^n}\right)_{\omega=\omega_0}. \tag{4.2.22}$$

The cubic and higher-order terms are negligible for a small spectral width. The coefficient β_2 denotes propagation regime [19]: the normal-dispersion regime for positive β_2 (long-wavelength spectral components travel faster than short-wavelength components), the anomalous-dispersion regime for negative β_2.
Substituting the Taylor expansion (4.2.21) up to the second order to (4.2.19) and taking the inverse Fourier transform

$$A(z,t)=\frac{1}{2\pi}\int_{-\infty}^{\infty}\tilde{A}(z,\omega-\omega_0)\exp[-i(\omega-\omega_0)t]d\omega \tag{4.2.23}$$

we obtain

$$\frac{\partial A}{\partial z}=-\beta_1\frac{\partial A}{\partial t}-\frac{i}{2}\beta_2\frac{\partial^2 A}{\partial t^2}+i\Delta\beta A. \tag{4.2.24}$$

After transformation (employing the co-moving frame)

$$T = t - \beta_1 z, \tag{4.2.25}$$

the propagation equation in the simplest form can be written as

$$\frac{\partial A}{\partial z} = -\frac{\alpha}{2} A - \frac{i}{2}\beta_2 \frac{\partial^2 A}{\partial T^2} + i\gamma |A|^2 A, \tag{4.2.26}$$

where α and γ were introduced by evaluating $\Delta\beta$ from the first-order perturbation theory. An interpretation of these parameters is following: α is the attenuation coefficient (negligible for short fibres) and γ is the nonlinear coefficient given by

$$\gamma = \frac{n_2 \omega_0}{c A_{\text{eff}}}, \tag{4.2.27}$$

where n_2 is the nonlinear refractive index and A_{eff} is the effective core area. Equation (4.2.26) is usually called the nonlinear Schrödinger equation.
This equation can be generalized for pulse widths ≤ 0.1 ps. The spectrum of such pulses is wide enough to employ Raman scattering between spectral components of the pulse. Further, due to the wider spectrum, the third term in Taylor expansion (4.2.21) must be included and an assumption of the instantaneous nonlinear response is not justified. Hence, the propagation equations for this case is usually written in the form [20]

$$\begin{aligned}\frac{\partial A}{\partial z} = &-\frac{\alpha}{2} A - \frac{i}{2}\beta_2 \frac{\partial^2 A}{\partial T^2} + \frac{1}{6}\beta_3 \frac{\partial^3 A}{\partial T^3} \\ &+ i(1-f_R)\gamma |A|^2 A + i\gamma f_R A(z,T) \int_{-\infty}^{T} h_R(T-T') |A(z,T')|^2 \, dT',\end{aligned} \tag{4.2.28}$$

where $f_R = 0.18$ is the fraction of the Raman contribution to the refractive index and $h_R(T)$ is the Raman response function

$$h_R(T) = \frac{\tau_1^2 + \tau_2^2}{\tau_1 \tau_2^2} \exp\left(-\frac{T}{\tau_2}\right) \sin\left(\frac{T}{\tau_1}\right), \tag{4.2.29}$$

with $\tau_1 = 12.2$ fs and $\tau_2 = 32$ fs. The last term on the right-hand side of (4.2.28) is referred as the self-frequency shift (or intrapulse Raman scattering), when short-wavelength frequency components in the pulse spectrum act as a pump for long-wavelength components. Equation (4.2.28) is usually called the generalized nonlinear Schrödinger equation. A rigorous approach to derivation of this equation based on a quantum-mechanical approach is presented in [21] and [22].
Equations (4.2.26) and (4.2.28) have analytical solutions only for special cases. Generally, numerical methods must be used, mostly the split-step Fourier method discussed in Appendix A.

4.3 Group-velocity dispersion (GVD)

4.3.1 Pulse broadening due to GVD

Let us introduce a normalized amplitude $U(z,T)$ by prescription

$$A(z,T) = \sqrt{P_0}\exp(-\alpha z/2)U(z,T), \tag{4.3.1}$$

where P_0 is the peak power of the input pulse and the exponential factor represents the fibre loss. By neglecting the nonlinear effects, the propagation equation (4.2.26) for the normalized amplitude $U(z,T)$ is of the form

$$\frac{\partial U}{\partial z} = -\frac{i}{2}\beta_2\frac{\partial^2 U}{\partial T^2}. \tag{4.3.2}$$

Equation (4.3.2) can be solved analytically. Using the Fourier transform in time it has a form of an ordinary differential equation

$$\frac{\partial \tilde{U}}{\partial z} = \frac{i}{2}\beta_2\omega^2\tilde{U}, \tag{4.3.3}$$

where $\tilde{U}(z,\omega)$ denotes the Fourier transform of $U(z,T)$. The solution is

$$\tilde{U}(z,\omega) = \tilde{U}(0,\omega)\exp\left(\frac{i}{2}\beta_2\omega^2 z\right). \tag{4.3.4}$$

The amplitude $U(z,T)$ is then given by the inverse Fourier transform of this solution.
Let us consider the input unchirped pulse of a Gaussian profile

$$U(0,T) = \exp\left(-\frac{T^2}{2T_0^2}\right), \tag{4.3.5}$$

where the width parameter T_0 is the half-width at $1/e$ of maximum. For a Gaussian profile, this parameter is coupled with the full width at half maximum T_{FWHM} by the relation

$$T_{\mathrm{FWHM}} \simeq 1.665T_0. \tag{4.3.6}$$

Taking the inverse Fourier transform of the solution (4.3.4) we have

$$U(z,T) = \frac{T_0^2}{T_0^2 - i\beta_2 z}\exp\left(-\frac{T^2}{2(T_0^2 - i\beta_2 z)}\right). \tag{4.3.7}$$

This solution is also a Gaussian pulse, but its half-width at $1/e$ of maximum after propagating a distance z is given by

$$T_1 = T_0\sqrt{1+(z/L_D)^2}, \tag{4.3.8}$$

where

$$L_D = \frac{T_0^2}{|\beta_2|} \tag{4.3.9}$$

is the dispersion length, characterizing dispersion properties during the propagation. It denotes the length where the Gaussian pulse broadens $\sqrt{2}$ - times. Thus, independently on the sign of β_2, the GVD effect leads to a broadening of the initially unchirped pulse.
Other feature of the solution (4.3.7) is that although the initial pulse was unchirped, during propagation it becomes chirped. The instantaneous frequency across the pulse changes and differs from its central frequency according to formula [19]

$$\delta\omega = \frac{2\,\mathrm{sgn}(\beta_2)(z/L_D)}{1+(z/L_D)^2}\frac{T}{T_0^2}. \tag{4.3.10}$$

This chirp is linear across the pulse and depends on the sign of β_2. In the normal-dispersion regime the chirp increases linearly across the pulse, in the anomalous-dispersion regime it decreases.
The evolution of the pulse chirp and width is different when the pulse has an initial chirp. Let us concern the input Gaussian pulse with a linear initial chirp given by the chirp parameter C:

$$U(0,T) = \exp\left[-\frac{(1+iC)}{2}\frac{T^2}{T_0^2}\right]. \tag{4.3.11}$$

The solution of (4.3.2) for such a pulse is analogous to the solution for an initially unchirped pulse, however, the formula for the half-width at $1/e$ of maximum after propagating a distance z takes the form

$$T_1 = T_0\sqrt{\left(1+\frac{C\beta_2 z}{T_0^2}\right)^2+\left(\frac{\beta_2 z}{T_0^2}\right)^2}. \tag{4.3.12}$$

The pulse-width evolution now depends on the sign of the product $C\beta_2$. In the case of $C\beta_2 > 0$, the pulse broadens monotonically like for the pulse without an initial chirp. On the other hand, a negative sign of the product $C\beta_2$ (opposite directions of the initial chirp and the chirp induced by GVD) causes an initial narrowing of the pulse. The narrowest pulse width occurs at the distance where the GVD-induced chirp cancels the initial chirp. After that, the pulse broadens monotonically.
The pulses emitted from the fibre lasers working in soliton regime (see Secs. 4.5 and 4.6) have a hyperbolic-secant profile [19]

$$U(0,T) = \mathrm{sech}\left(\frac{T}{T_0}\right)\exp\left(-\frac{iCT^2}{2T_0^2}\right), \tag{4.3.13}$$

where the width parameter T_0 is related to the full width at half-maximum T_{FWHM} by the relation

$$T_{FWHM} \simeq 1.763 T_0 . \tag{4.3.14}$$

The solution of (4.3.2) for hyperbolic-secant pulses can not be carried out in the closed form (unlike Gaussian pulses), but the qualitatively features of the pulse broadening are the same.

4.3.2 Dispersion of the third order

In cases when the pulse wavelength is near the zero-dispersion wavelength (where $\beta_2 \simeq 0$), the third-order term with β_3 in the expansion of $\beta(\omega)$ comes to importance. It must be taken into an account for pulse widths ≤ 0.1 ps, too. The propagation equation is then of the form

$$\frac{\partial U}{\partial z} = -\frac{i}{2}\beta_2 \frac{\partial^2 U}{\partial T^2} + \frac{1}{6}\beta_3 \frac{\partial^3 U}{\partial T^3} . \tag{4.3.15}$$

This equation can be solved similarly to (4.3.2) using the Fourier transform [19]. As a result, β_3 term contributes to a broadening of the pulse independently on the relative sign of both β_3 and C. Much more important conclusion from accounting β_3 to the propagation equation is that third-order dispersion leads to the distortion of the pulse shape, as described in [19]. The pulse becomes asymmetric with an oscillatory structure at one of its edges. In the case of $\beta_3 > 0$, the trailing edge develops oscillations while the opposite appears when $\beta_3 < 0$. The oscillations are significantly deep only close to the zero-dispersion wavelength.
To characterize the effect of third-order dispersion, the dispersion length related to third-order dispersion can be introduced by the relation

$$L_D' = \frac{T_0^3}{|\beta_3|} . \tag{4.3.16}$$

The effects of third-order dispersion are significant only for $L_D' \leq L_D$.

4.3.3 Dispersion parameter D and dispersion slope S

Dispersion features of the fibre are commonly characterized by the parameters D and S. The parameter S is related to D by the prescription

$$S = \frac{dD}{d\lambda} . \tag{4.3.17}$$

These parameters are coupled with β_2 and β_3 by relations

$$\beta_2 = -\frac{\lambda^2}{2\pi c} D , \tag{4.3.18}$$

$$\beta_3 = \left(\frac{\lambda}{2\pi c}\right)^2 \left(\lambda^2 S + 2\lambda D\right). \tag{4.3.19}$$

Parameters D and S are widely used in technical literature [7].

4.4 Self-phase modulation (SPM)

4.4.1 Spectral broadening

After substituting the normalized amplitude defined by (4.3.1) and neglecting the GVD, the propagation equation (4.2.26) has the form [19]

$$\frac{\partial U}{\partial z} = \frac{i}{L_{NL}} e^{-\alpha z} |U|^2 U, \tag{4.4.1}$$

where L_{NL} is the nonlinear length introduced by

$$L_{NL} = \frac{1}{\gamma P_0}. \tag{4.4.2}$$

Equation (4.4.1) is an ordinary differential equation with solution

$$U(z,T) = U(0,T)\exp[i\Phi_{NL}(z,T)]. \tag{4.4.3}$$

The nonlinear phase shift is given by

$$\Phi_{NL}(z,T) = |U(0,T)|^2 (z_{eff} / L_{NL}), \tag{4.4.4}$$

where

$$z_{eff} = \frac{1}{\alpha}[1 - e^{-\alpha z}]. \tag{4.4.5}$$

The phase shift (4.4.4) depends on time, which is why the instantaneous frequency varies across the pulse. The difference between the instantaneous frequency and the central frequency ω_0 is given by

$$\delta\omega(z,T) = -\frac{\partial \Phi_{NL}(z,T)}{\partial T} = -\frac{\partial |U(0,T)|^2}{\partial T} \frac{z_{eff}}{L_{NL}}. \tag{4.4.6}$$

The time dependence of $\delta\omega(z,T)$ can be understood as a frequency chirp. Assuming a Gaussian initial pulse given by (4.3.5), the SPM-induced frequency chirp is

$$\delta\omega(T) = \frac{z_{eff}}{L_{NL}} \frac{2T}{T_0^2} \exp\left(-\frac{T^2}{T_0^2}\right). \tag{4.4.7}$$

This SPM-induced frequency chirp is positive and linear across the central part of the pulse. The chirp increases in magnitude with the propagation length which means that SPM creates new frequency components continuously during the pulse propagation.
The actual pulse spectrum is to be calculated from the relation

$$S(\omega)=\left|\tilde{U}(z,\omega)\right|^2=\left|\int_{-\infty}^{\infty}U(0,T)\exp[i\Phi_{NL}(z,T)+i(\omega-\omega_0)T]dT\right|^2, \tag{4.4.8}$$

where $\tilde{U}(z,\omega)$ denotes the Fourier transform of $U(z,T)$.
Spectrum broadened by SPM has an oscillatory structure and peaks at the edges of the spectrum are the most intense. Number of spectral peaks M is related to the propagation distance by the relation

$$\gamma P_0 z_{eff}\simeq\left(M-\frac{1}{2}\right)\pi. \tag{4.4.9}$$

The oscillary structure of the spectrum can be explained from the time dependence of the chirp [19]. The same value of the chirp occurs at two distinct values of T. These two points represent two waves with the same frequency and different phases, which can interfere. This interference can be constructive of destructive in dependence on the relative phase difference between the two waves. Such interference results into the multipeak structure of the SPM-broadened spectrum.

4.4.2 Effect of GVD

In order to account the GVD influence to SPM, let us introduce the normalized distance and time variables

$$\xi=\frac{z}{L_D}, \tag{4.4.10}$$

$$\tau=\frac{T}{T_0}. \tag{4.4.11}$$

After this substitution, the propagation equation is of the form

$$\frac{\partial U}{\partial\xi}=-\frac{i}{2}\operatorname{sgn}(\beta_2)\frac{\partial^2U}{\partial\tau^2}+iN^2e^{-\alpha z}|U|^2U, \tag{4.4.12}$$

where

$$N^2=\frac{L_D}{L_{NL}}=\frac{\gamma P_0T_0^2}{|\beta_2|}. \tag{4.4.13}$$

The parameter N governs the relative significance of nonlinearity and dispersion. SPM dominates above GVD for $N\gg1$ while the opposite occurs for $N\ll1$.

Equation (4.4.12) must be solved numerically, commonly using the split-step Fourier method. Assuming $N = 1$ and neglecting fibre loss, the numerical solution of (4.4.12) is characterized in [19] as follows: in the normal-dispersion regime, a broadening of the initially unchirped Gaussian pulse is faster than in the case of no SPM (SPM produces new red-shifted frequency components at the leading edge and blue-shifted frequency components at the trailing edge of the pulse; the red components travel faster than the blue components, so the pulse broadens more rapidly in conclusion). In the anomalous-dispersion regime, behaviour of the initially unchirped Gaussian pulse is different. The initial broadening is much slower and after 4 L_D the steady-state appears. The SPM-induced chirp is positive, while the GVD-induced chirp is negative, so they can cancel each other in the central part of the pulse. The propagation of the pulse in the anomalous-dispersion regime is coupled with soliton effects, which are discussed in Sec. 4.5.

4.4.3 Effect of third-order dispersion

The propagation of the pulse with a small temporal width (≤ 0.1 ps) or near the zero-dispersion wavelength is described by the equation

$$\frac{\partial U}{\partial \xi'} = \frac{1}{6}\operatorname{sgn}(\beta_3)\frac{\partial^3 U}{\partial \tau^3} + i\bar{N}^2 e^{-\alpha z}|U|^2 U, \tag{4.4.14}$$

where

$$\xi' = \frac{z}{L_D'} \tag{4.4.15}$$

and

$$\bar{N}^2 = \frac{L_D'}{L_{NL}} = \frac{\gamma P_0 T_0^3}{|\beta_3|}. \tag{4.4.16}$$

Let us assume $\bar{N} \gg 1$. In the case of an initially unchirped Gaussian pulse and $\beta_3 > 0$, the effect of third-order dispersion leads to an asymmetric shape of the pulse with deep oscillation near the trailing edge [19]. Due to large temporal oscillations, the first term on the right-hand side of (4.4.14) becomes more significant because of a large third derivative of U.

4.5 Optical solitons

The soliton propagation is a result of interplay between SPM and anomalous GVD. The propagation equation in the normalized form (4.4.12) for anomalous dispersion and lossless case

$$\frac{\partial U}{\partial \xi} = \frac{i}{2}\frac{\partial^2 U}{\partial \tau^2} + iN^2|U|^2 U \tag{4.5.1}$$

can be solved by the inverse scattering method [19].

Using the substitution

$$u = NU = \sqrt{\frac{\gamma T_0^2}{|\beta_2|}} A, \tag{4.5.2}$$

equation (4.5.1) is of the form

$$i\frac{\partial u}{\partial \xi} + \frac{1}{2}\frac{\partial^2 u}{\partial \tau^2} + |u|^2 u = 0. \tag{4.5.3}$$

The steady-state solution obtained by the inverse scattering method corresponding to $N = 1$ is called the fundamental soliton. It can be written as

$$u(\xi, \tau) = \mathrm{sech}(\tau)\exp(i\xi/2). \tag{4.5.4}$$

Thus, when the peak power and the pulse width are such as $N = 1$ and the hyperbolic secant pulse is launched into the lossless fibre, the pulse will propagate without change of its shape.
The higher-order solitons are arisen when the pulse shape at $\xi = 0$ is

$$u(0, \tau) = N\mathrm{sech}(\tau), \tag{4.5.5}$$

where $N > 1$ and it is an integer. The higher-order solitons do not maintain their shape during propagation. Nevertheless, their evolution is periodic with the soliton period

$$z_0 = \frac{\pi}{2} L_D. \tag{4.5.6}$$

The time evolution of the Nth-order soliton during one soliton period is following: first, the pulse is contracted, then split into N fundamental solitons at the half of the soliton period and merged into the original shape at the end of the period. The initial narrowing of the higher-order solitons can be used for the pulse compression.
The soliton regime of the propagation is widely used in the fibre lasers [23] and optical communications [19]. The soliton lasers are discussed in Sec. 4.6.

4.6 Ultrafast fibre lasers and similaritons

4.6.1 Introduction

Fibre lasers are compact, robust, inexpensive and stable. Variability of fibre components leads to minimizing the need of bulk optics and mechanical alignment. In addition with mode-locking, they can generate a train of pulses and therefore it is possible to use them in optical communication systems as well as in supercontinuum generation. Fibres doped by Er^{3+} are mostly used for amplification of the pulses in fibre lasers.
The operation regime of the fibre laser must eliminate the detrimental influence of excessive nonlinearity. Therefore, nonlinearity and dispersive effects must be balanced. Mutual cancelling of nonlinearity and anomalous-dispersion effects leads to the

propagation of solitons (hyperbolic secant profile of the pulse shape). The soliton regime of the laser can be proven by spectral measuring of the propagating pulse. When the fibre laser works in the soliton regime, so called Kelly's sidebands occur in the spectrum.
Kelly's spectral sidebands are consequences of perturbations like the output coupler, filtering or amplifying. The pulse circulates in the cavity, so these perturbations become periodical. The perturbed soliton emits dispersive radiation while reshaping back into the soliton shape [23]. Waves of this dispersive radiation have a dispersion relation

$$k_{\text{disp}} = -\frac{|\beta_2|}{2}\Delta\omega^2, \tag{4.6.1}$$

where $\Delta\omega$ is the frequency offset from the central frequency. This dispersive wave is emitted each period L (the laser length).
The phase-matching between the dispersive wave and the soliton wave occurs when

$$L\left(k_s - k_{\text{disp}}\right) = 2\pi m, \tag{4.6.2}$$

where m is an integer and

$$k_s = \frac{|\beta_2|}{2T_0^2}. \tag{4.6.3}$$

Solving the relation (4.6.2), corresponding $\Delta\omega$ is to be found:

$$\Delta\omega = \pm\frac{1}{T_0}\sqrt{m\frac{8z_0}{L} - 1}, \tag{4.6.4}$$

where z_0 stands for the soliton period introduced by (4.5.6). The Kelly's sidebands occur in the pulse shape as a pedestal under the pulse, limiting the shortest available pulse width.
Another limitation of soliton lasers is a limitation of pulse peak power, which can be derived from the soliton area theorem [23]. If we write the soliton shape as

$$A(t) = A_0\,\text{sech}\left(\frac{t}{T_0}\right), \tag{4.6.5}$$

the soliton area must satisfy the following relation:

$$A_0 T_0 = \sqrt{\frac{|\beta_2|\lambda A_{\text{eff}}}{2\pi n_2}}, \tag{4.6.6}$$

where n_2 is the nonlinear refractive index, A_{eff} is the effective core area and λ is the operation wavelength of the laser.
Assuming hyperbolic secant shape of the soliton pulse, relation between nonlinearity and the peak power is

$$\gamma|A_0|^2 \simeq 0.6\pi. \tag{4.6.7}$$

If the peak power exceeds this limitation, the single pulse in the cavity will decay into multiple pulses without defined timing. It can be shown that energy of the pulse is limited to be up to 0.1 nJ [24].

4.6.2 Actively mode-locked soliton fibre lasers

Active mode-locking in fibre lasers can be obtained by a high-speed electro-optic modulator placed into the cavity [23]. These lasers are widely used as light sources in optical communication systems (time-division multiplexing and wavelength-division multiplexing), because of a defined repetition rate of the output pulses. This repetition rate can be higher than 1 GHz.
In optical communication systems, the pulse-to-pulse energy stability is required. Unfortunately, the relaxation time of the Er^{3+} (~ 10 ms) is slow in comparison with the pulse spacing (~ 1 ns), so that it cannot stabilize the pulse energy variations.
One way how to stabilize the pulse energy is inserting a spectral filter into the cavity. SPM generates more broadened spectrum for a pulse with a higher intensity, so that loss in the filter is higher than for a lower-intensity pulse. Another way is using the effect of nonlinear polarization rotation, as described below in the section concerning passively mode-locked lasers.

4.6.3 Passively mode-locked soliton fibre lasers

In passively mode-locked lasers, the cavity loss is modulated without an external modulator. The lasers can be self-starting (a pulse is built up from a noise). One possibility how to modulate the cavity loss is nonlinear polarization rotation, using nonlinear effects in the fibre. The principle of this method is the intensity-dependent rotation of an elliptical polarization of the pulse during its propagation in a fibre (see Fig. 4.6.1)

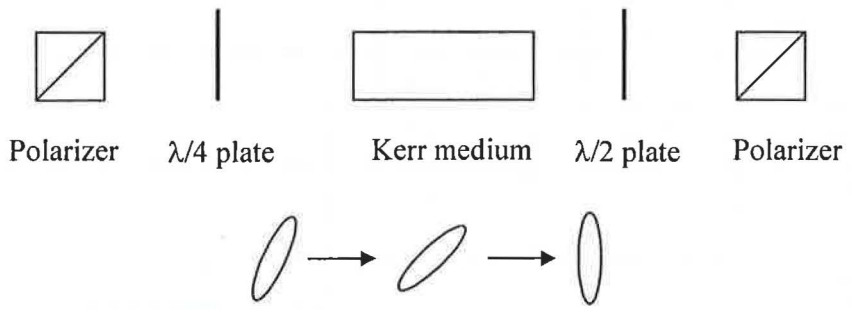

Fig. 4.6.1 The setup for a pulse shortening using nonlinear-polarization rotation (after [23]). Evolution of the elliptical polarization of the pulse is shown.

An initial linearly polarized pulse is transformed to an elliptic polarized pulse by a quarter-wave plate. In the Kerr medium, the rotation of the principal axes of the polarization ellipse is intensity-dependent. The peak of the pulse rotates more than wings due to a higher intensity. A half-wave plate orients the pulse polarization such that the peak of the pulse passes through the polarizer, while the wings are suppressed.

In the slowly-varying envelope approximation, the propagation of the pulse in the passively mode-locked laser can be described by the Master equation [23]:

$$\left[-i\psi + g - \alpha + \left(\frac{g}{\Omega_g} + \frac{i}{2}\beta_2 L\right)\frac{\partial^2}{\partial t^2} + \left(-i\delta + S\right)|u|^2\right]u = 0, \tag{4.6.8}$$

where $u(t)$ is the complex amplitude of the slowly varying envelope, ψ is the net linear phase shift, g is the laser gain, α is the loss per one pass and S represents the saturable absorber. Parameter δ is defined as

$$\delta = \frac{2\pi n_2 L}{\lambda A_{\text{eff}}}. \tag{4.6.9}$$

The exact solution of (4.6.8) is a chirped hyberbolic-secant pulse.

4.7 OTDM and WDM communication systems

4.7.1 OTDM systems

Time division multiplexing is based on dividing a high-speed digital data stream into more slower-speed data streams, as shown in Fig. 4.7.1. Time intervals in the output stream are called time slots.

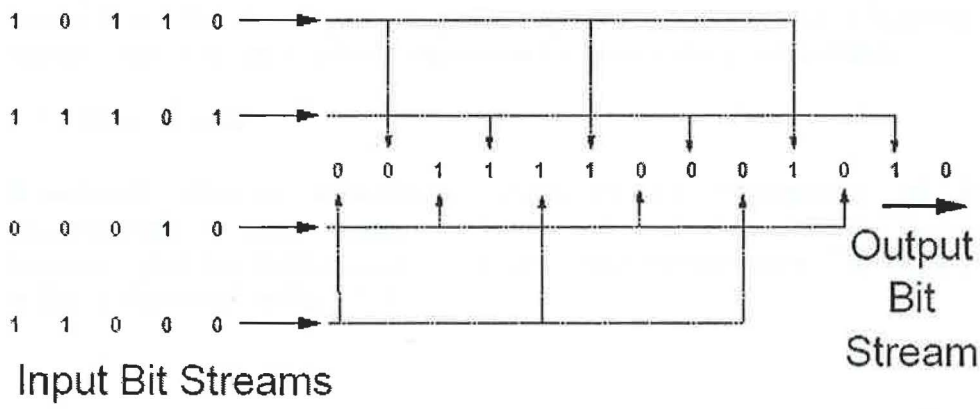

Fig. 4.7.1 Principle of time division multiplexing (after [3]). Each of input bit streams is assigned to every fourth bit in a high-speed output bit stream. The input streams must be exactly synchronized to the higher-speed output stream.

The fastest electronic modulators can produce bit rate up to 30 Gbps (gigabits per second). This limitation leaded to using an optical signal rather than an electronic signal. Optical time division multiplexing (OTDM) systems based on the soliton transmission can reached a bit rate of about 200 Gbps. A concept of an OTDM transmitter is illustrated in Fig. 4.7.2.

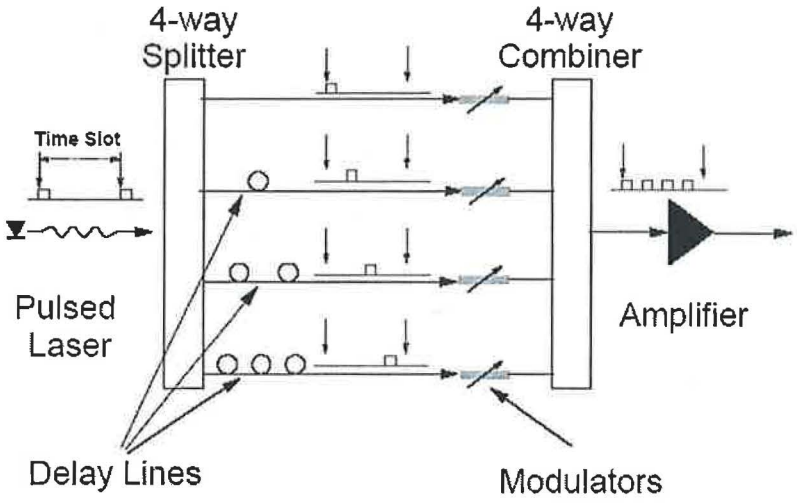

Fig. 4.7.2 Concept of OTDM transmitter (after [3]).

The logical "1" is realized by the pulse in the time slot, while the time slot is dark for the logical "0". The laser signal is split into four lines and a fixed time delay between the lines is provided by fibre loops. Each line is modulated to carry its own information. Then, the four lines are combined together into the output stream, which is amplified to reach an appropriate strength for the transmission and detection.
A synchronizing clock signal must be transmitted with the data stream and used for data recovery in the receiver. The clock signal is mostly realized by a tunable laser. However, using of a supercontinuum as a tunable otical clock translator can save the cost of the tunable laser. The clock signal at required wavelength can be extracted from the SC using a tunable filter. This application is demostrated experimentally in this thesis.

4.7.2 WDM systems

Wavelength division multiplexing comprises the transmission of the signals simultaneously in more separated and independent spectral channels. It is identical to frequency division multiplexing in TV and radio transmissions. The basic principle of WDM is illustrated in Fig. 4.7.3.

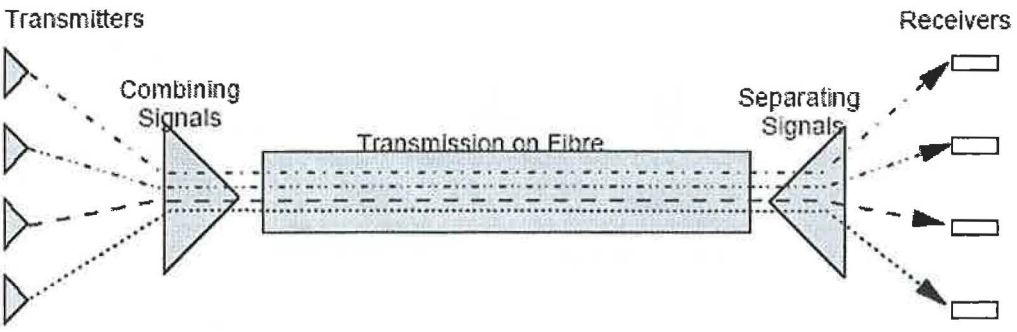

Fig. 4.7.3 Principle of WDM system (after [3]).

The light source for the WDM system can be realized by lasers at the fixed wavelengths, each for one spectral channel. However, the usage of a multiwavelength source would considerably simplify the WDM source construction. The configuration of the WDM source is shown in Fig. 4.7.4.

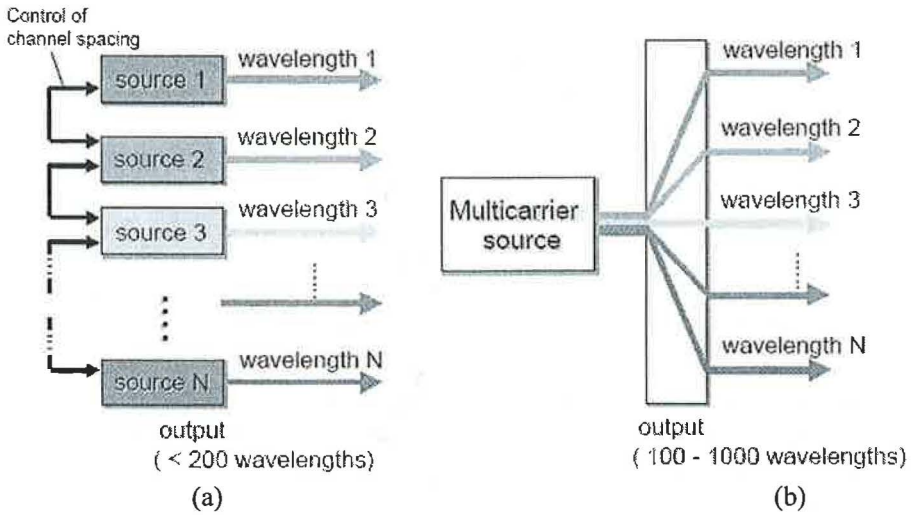

Fig. 4.7.4 Configuration of the WDM source (a) with more separated sources, (b) with one multiwavelength source (after [14]).

Supercontinuum generation in combination with an optical filter or multiplexor can be used as a multiwavelength source. A high degree of coherence of SC can considerably increase the signal-to-noise ratio in the spectral channels. The desired properties of SC are a good flatness (in order to have a uniform intensity in all spectral channels) and a high signal-to-noise ratio. Fig. 4.7.5 illustrates the construction of the SC-based WDM source.

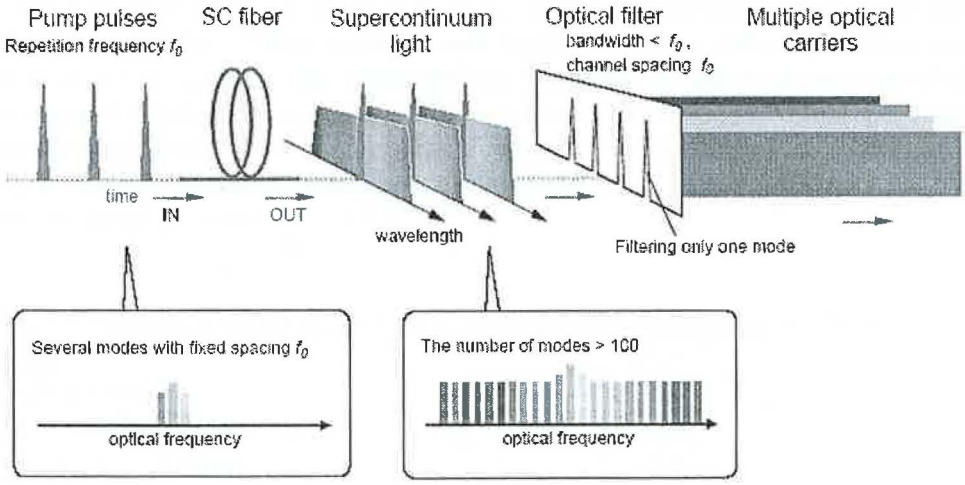

Fig. 4.7.5 Construction of the WDM source using supercontinuum (after [14]).

In real applications, it is necessary to use the pulse laser with a high and exactly defined repetition rate as a source of pulses.

5. Experimental and numerical results

5.1 Experimental equipment used for measurements

A passively mode-locked sub-picosecond fibre laser working in a soliton regime was used as a source of pulses. The central wavelength of the laser was around 1533 nm. In the soliton regime, significant Kelly's sidebands were observable in the spectrum. The cavity loss of the laser was managed by the nonlinear polarization rotation (described in Sec. 4.6.3). The laser was constructed at Guided-wave Photonics Department of Institute of Radio Engineering and Electronics. The signal from the laser was too weak to measure the pulse width with the autocorrelator. The 3-dB spectral width of the output pulse was around 4 nm. The basic repetition rate of the laser (determined by the cavity length) was 5.67 MHz and the number of pulses in one period was 28. In the schemes of the experimental setup, this laser is denoted as PMLFRL.

The pulses from this laser were amplified in the erbium-doped fibre amplifier (produced by INO), which was suitable for amplifying short pulses with a high peak power, probably due to a large field diameter of an active fibre. In typical experimental conditions the average output power from the amplifier was 4 – 20 mW, the FWHM of the output pulses varied in the range 0.5 – 1 ps and peak powers were between 80 and 640 W.

Another laser used in our experiments was a tunable passively-mode locked laser TMLL-1550 (produced by U2T). The repetition rate could be tuned around 10 GHz. The regime of the laser depended critically on a driving current of the laser, adjusted repetition rate and central wavelength. Due to a lower peak power of the output pulses, they could be amplified in the erbium-doped fibre amplifier (Keopsys) with the highest output average power around 20 dBm (100 mW). This amplifier had an active fibre with a small field diameter. Therefore, it was not suitable for the amplification of ultrashort pulses with a high peak power.

A 10-m microstructured optical fibre used in our experiments was described in Chapter 2. Its parameters at wavelengths used in our experiments were: the nonlinear coefficient $\gamma = 11\ (\mathrm{W \cdot km})^{-1}$, the dispersion parameter $D = -0.85$ ps/(nm·km), the dispersion slope $S = 0.015$ ps/(nm^2·km). The fibre was in the normal-dispersion regime in all spectral parts of the generated SC. Three conventional highly-nonlinear fibres (HNLFs) were used as well in order to compare the supercontinua generated in the microstructured fibre and in conventional fibres. The fibres have different zero-dispersion wavelengths, which allowed comparing the features of supercontinua generated with various relative positions of the pump wavelength and the zero-dispersion wavelength. The parameters of the conventional fibres are given in Tabs. 5.1.1 – 5.1.3.

Tab. 5.1.1 Parameters of the HNLF with a zero-dispersion wavelength of 1529 m

Length	500 m
Cladding diameter	125 μm
Mode field diameter at 1550 nm	3.89 μm
Attenuation at 1550 nm	0.77 dB/km
Dispersion parameter D at 1550 nm	0.40 ps/(nm·km)
Dispersion slope S at 1550 nm	0.019 ps/(nm^2·km)
Zero-dispersion wavelength	1529 nm
Nonlinear coefficient γ at 1550 nm	11 $(\mathrm{W \cdot km})^{-1}$

Tab. 5.1.2 Parameters of the HNLF with a zero-dispersion wavelength of 1543 m

Length	500 m
Cladding diameter	125 μm
Mode field diameter at 1550 nm	3.88 μm
Attenuation at 1550 nm	0.76 dB/km
Dispersion parameter D at 1550 nm	0.14 ps/(nm·km)
Dispersion slope S at 1550 nm	0.019 ps/(nm^2·km)
Zero-dispersion wavelength	1543 nm
Nonlinear coefficient γ at 1550 nm	11 (W·km)$^{-1}$

Tab. 5.1.3 Parameters of the HNLF with a zero-dispersion wavelength of 1560 m

Length	1010 m
Cladding diameter	125 μm
Mode field diameter at 1550 nm	3.91 μm
Attenuation at 1550 nm	0.86 dB/km
Dispersion parameter D at 1550 nm	-0.15 ps/(nm·km)
Dispersion slope S at 1550 nm	0.016 ps/(nm^2·km)
Zero-dispersion wavelength	1560 nm
Nonlinear coefficient γ at 1550 nm	11 (W·km)$^{-1}$

The spectral slicing of the generated supercontinuum was performed by a tunable filter. Other tunable filters were used to suppress the amplified spontaneous emission from the amplifiers. The spectra were measured with an optical spectrum analyser with a resolution of 0.1 nm. It was necessary to monitor the spectra at several positions in the experimental setup (the output from the laser, the spectrum after amplification, the supercontinuum generated in a nonlinear fibre, at positions following the tunable filters). The fibre couplers with coupling ratio 90/10 and 99/1 were used for monitoring of the spectra. A four-channel optical switch was used in order to switch the outputs of the couplers to the optical spectrum analyser. Therefore, no manual disconnections of connectors were necessary.
The signal after the spectral slicing was amplified by an erbium-doped fibre amplifier (Keopsys) with the highest output average power around 10 dBm (10 mW).
The autocorrelation traces of pulses were measured with an autocorrelator using a second-harmonic generation.

5.2 Simulations of dependence of SC-properties on an initial chirp

Characteristics of a generated SC are strongly dependent on the chirp of the pulse launched into the nonlinear fibre. The linear initial chirp can be described by the parameter C in relations (4.3.11) or (4.3.13). The numerical simulations of the SC generation in a 10-m microstructured optical fibre (used in the experiments) for initial linear chirps with C = -10, -5, 0, 5 and 10 were carried out in order to investigate the SC generation for a wide range of initial chirps. The input pulses had a hyperbolic-secant shape according to (4.3.13). The parameters of the initial pulse were T_0 = 0.244 fs, λ = 1533 nm, P_0 = 640 W). Such pulses correspond to output pulses from the INO amplifier for a high amplification.
The computed spectra are shown in Fig. 5.2.1.

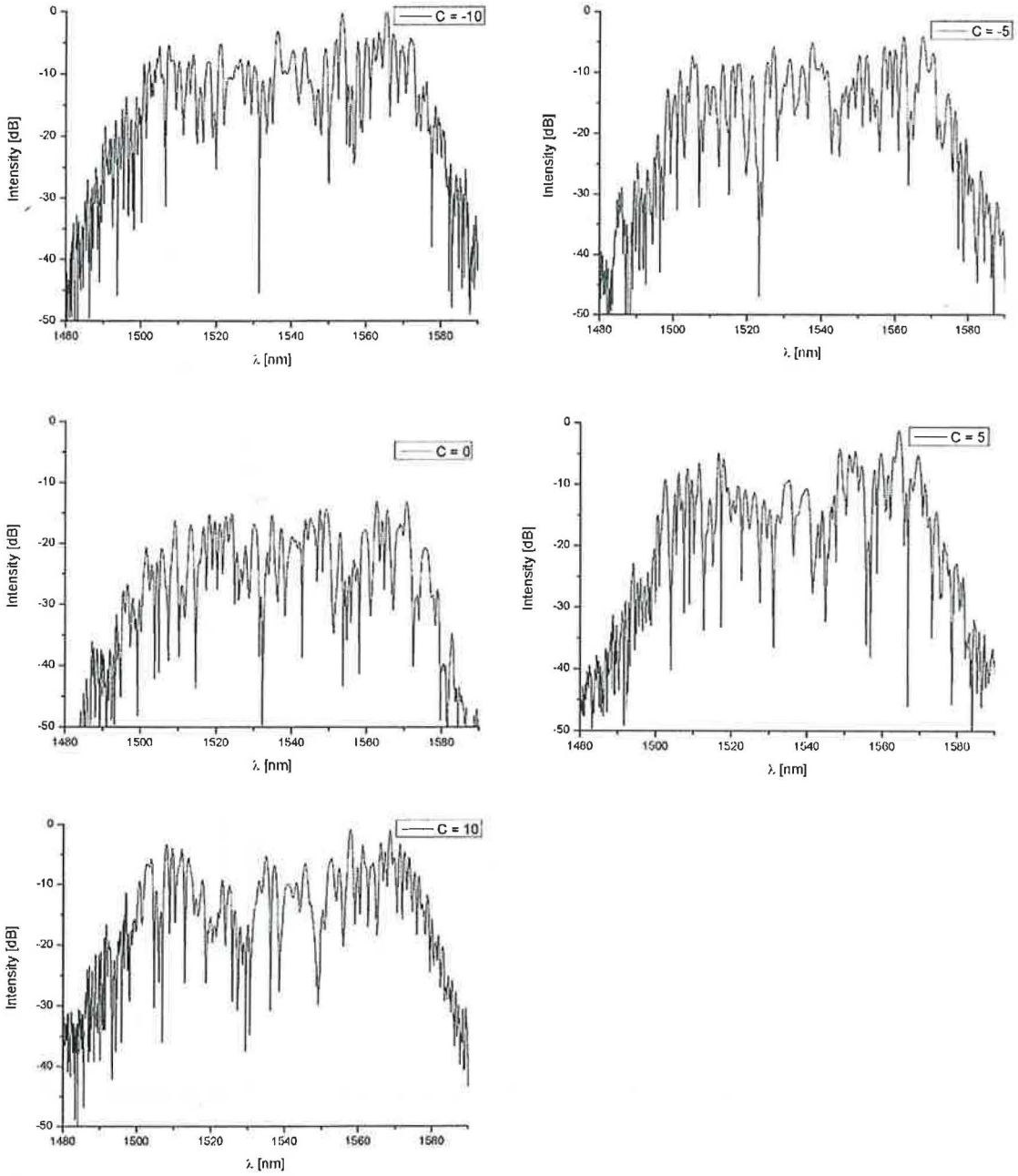

Fig. 5.2.1 Output spectra from MOF for C = -10, -5, 0, 5 and 10.

The spectra for positive values of C exhibit depletion in the central part. The SC generation is strongly suppressed for the case of $C = 0$. The bandwidth of SC does not depend significantly on the sign of C. An oscillatory structure of the spectra is a consequence of an interference of a train of short pulses.
Fig. 5.2.2 shows the evolution of the pulse shape during its propagation in the MOF.

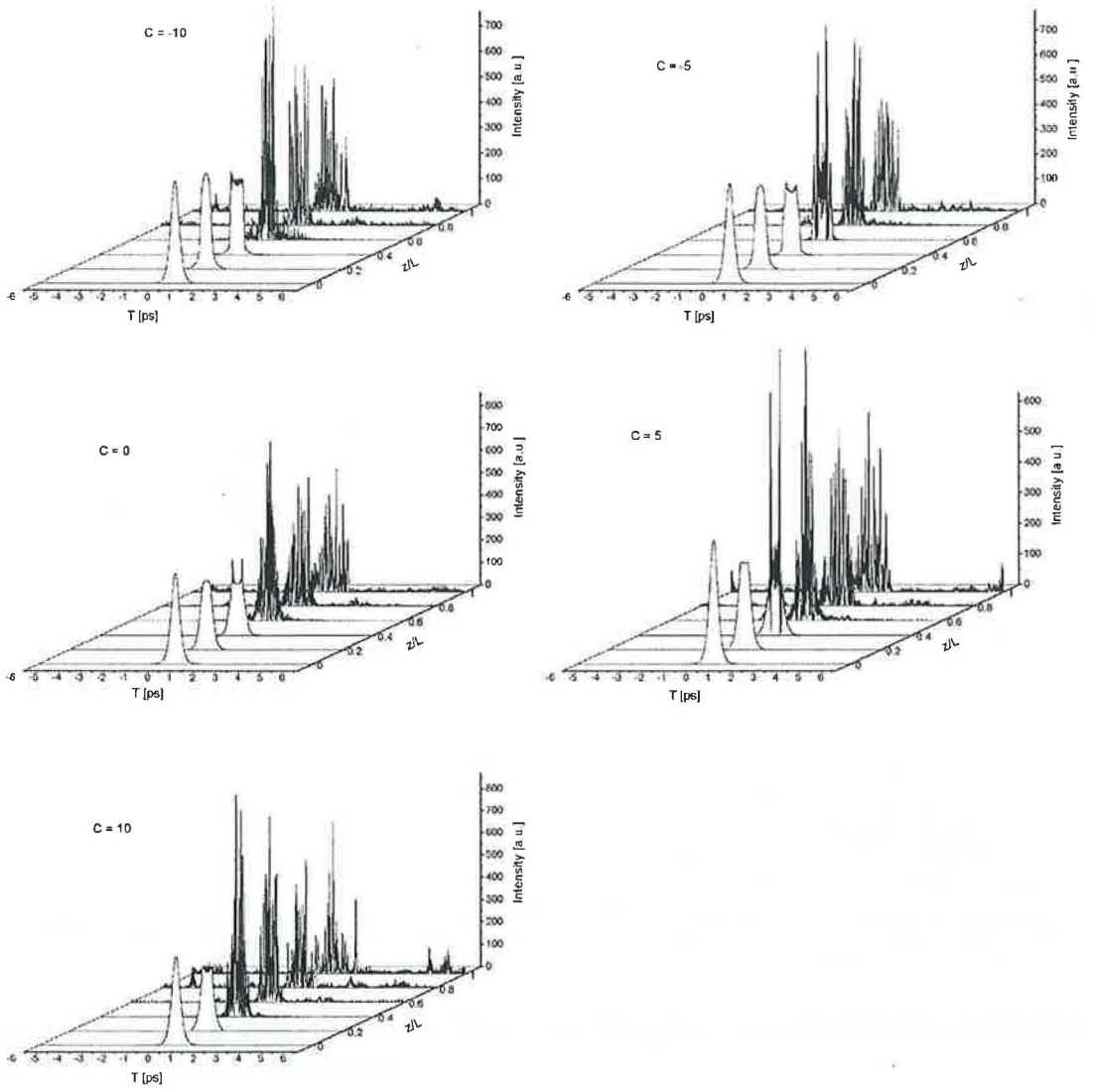

Fig. 5.2.2 Evolution of the pulse shape during the propagation for C = -10, -5, 0, 5 and 10.

The pulse shape exhibits decay due to interaction between a pulse chirp and third-order dispersion (the decay does not occur in the case of $\beta_3 = 0$). This satisfies the theoretical result that third-order dispersion can lead to the distortion of the pulse shape (see Sec. 4.3.2). When the initial pulse splits into the train of ultrashort pulses, the third derivative of the amplitude with respect to time becomes large locally, which causes further increasing the influence of third-order dispersion (see Sec. 4.4.3). The simulated evolutions of the pulse shape confirm these theoretical predictions. Fig. 5.2.2 shows the difference of the decay rate for opposite signs of the initial chirp. The pulse decays much more rapidly in the case of the positive initial chirp.

The width of the pulses in the pulse train after decay was estimated to be 15 – 20 fs. The usage of the slowly-varying envelope approximation for the description of such pulses is not quite correct. The direct integration of the Maxwell's equations (instead of the

nonlinear Schrödinger equation) would be a rigorous description of such ultrashort-pulse train. However, this approach is not presented in this thesis.
Further simulations were carried out to investigate the pulse decay in detail. Sequences of the decay are shown in Fig. 5.2.3 and 5.2.4.

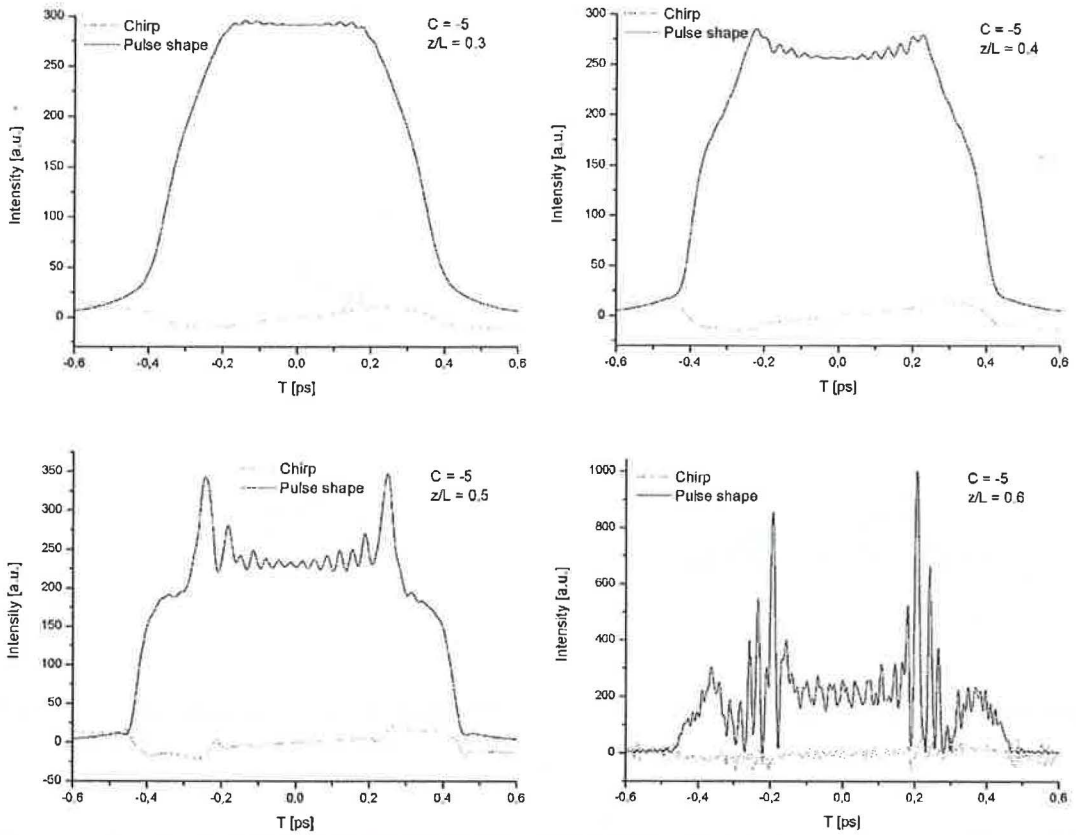

Fig. 5.2.3 Sequence of the pulse decay for C = -5. The pulse shape and chirp are plotted after z/L = 0.1, where L is the fibre length.

Several interesting features are worth noticing. The SPM-induced positive chirp described by (4.4.7) occurs very soon for both signs of the initial chirp. This chirp further develops to a more complex structure especially in the pulse edges and the decay phase is connected to the deformation of the chirp. The differences in the pulse-shape development for opposite signs of C are obvious. In the case of $C < 0$, the pulse shape acquires the rectangular-like shape with oscillations on the top of the pulse. These oscillations become deeper and the pulse edges increase their steepness during the propagation. The decay phase is connected to an appearance of significant peaks, which are observable in the decayed pulse, too. The case of $C > 0$ exhibits qualitatively different features. The oscillations in the central part of the pulse do not appear and the pulse edges are not steep. However, the peaks at the pulse edges appear as well.

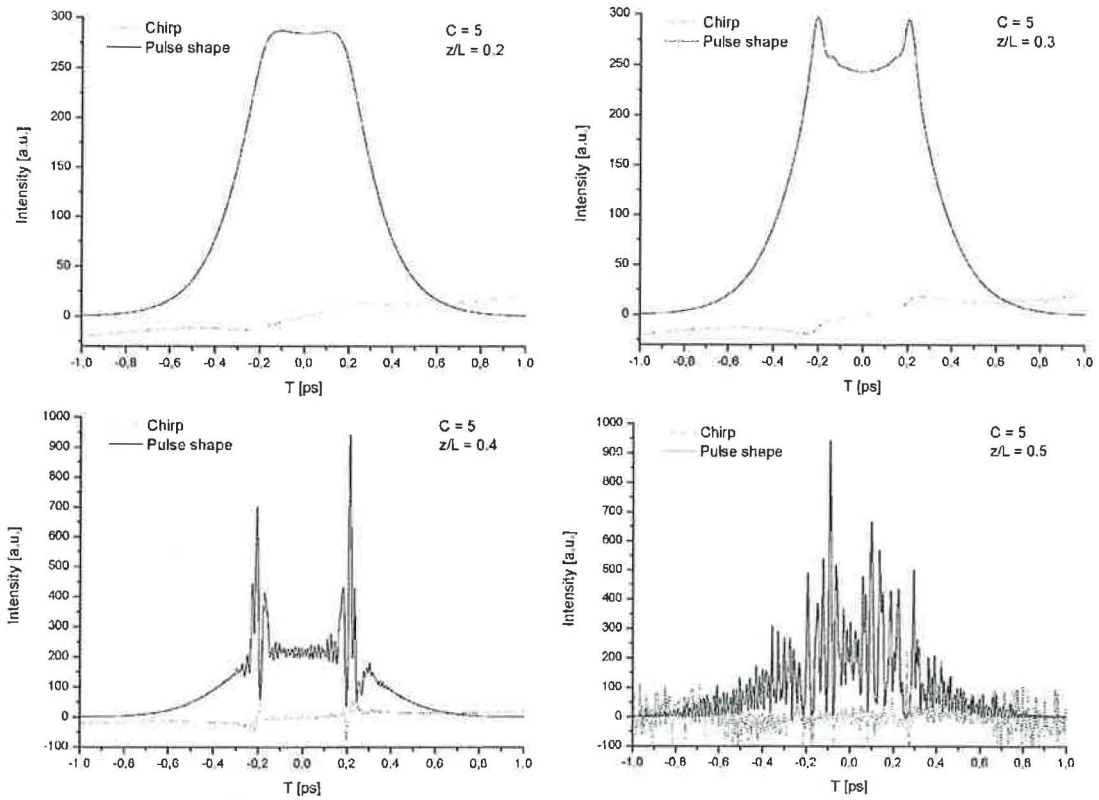

Fig. 5.2.4 Sequence of the pulse decay for $C = 5$. The pulse shape and chirp are plotted after $z/L = 0.1$, where L is the fibre length.

The simulated autocorrelation traces of the output from the MOF are plotted in Fig. 5.2.5. The extremely narrow peak is a consequence of the pulse decay. Due to a decrease of a coherence time, the narrow peak changes rapidly into a broad pedestal.

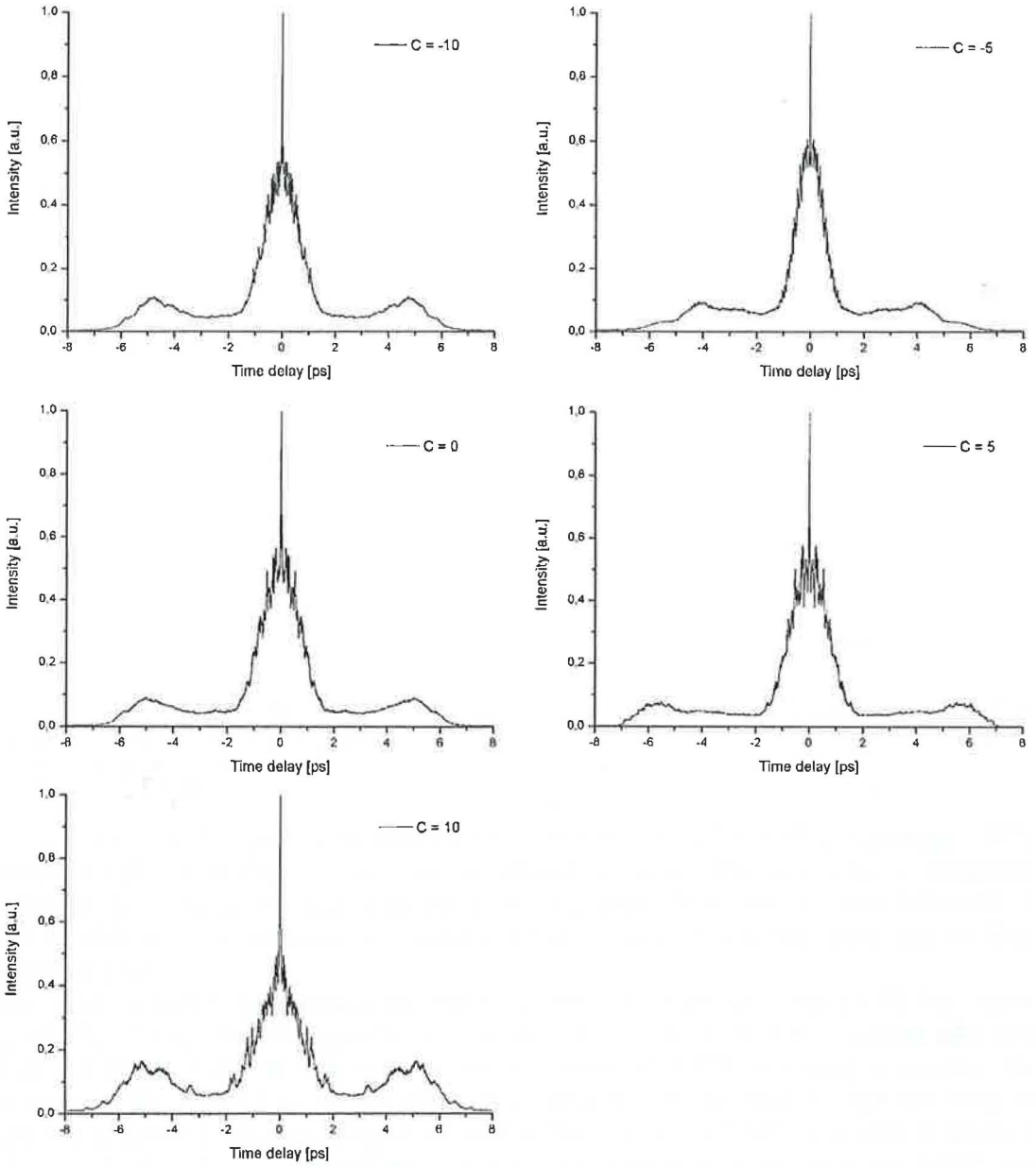

Fig. 5.2.5 Autocorrelation traces of the output from the MOF for C = -10, -5, 0, 5 and 10. Autocorrelation traces in simulations were computed according to [25].

5.3 Measurements of SC generation in microstructured fibre using a sub-picosecond laser

The experimental setup is shown in Fig. 5.3.1. As a pulse source, a sub-picosecond passively mode-locked fibre ring laser (PMLFRL) was used. The central wavelength of the PMLFRL was 1533 nm. The regime of the laser was monitored at an optical spectrum analyser (OSA) and the repetition rate was measured at a high-speed oscilloscope (OSC).

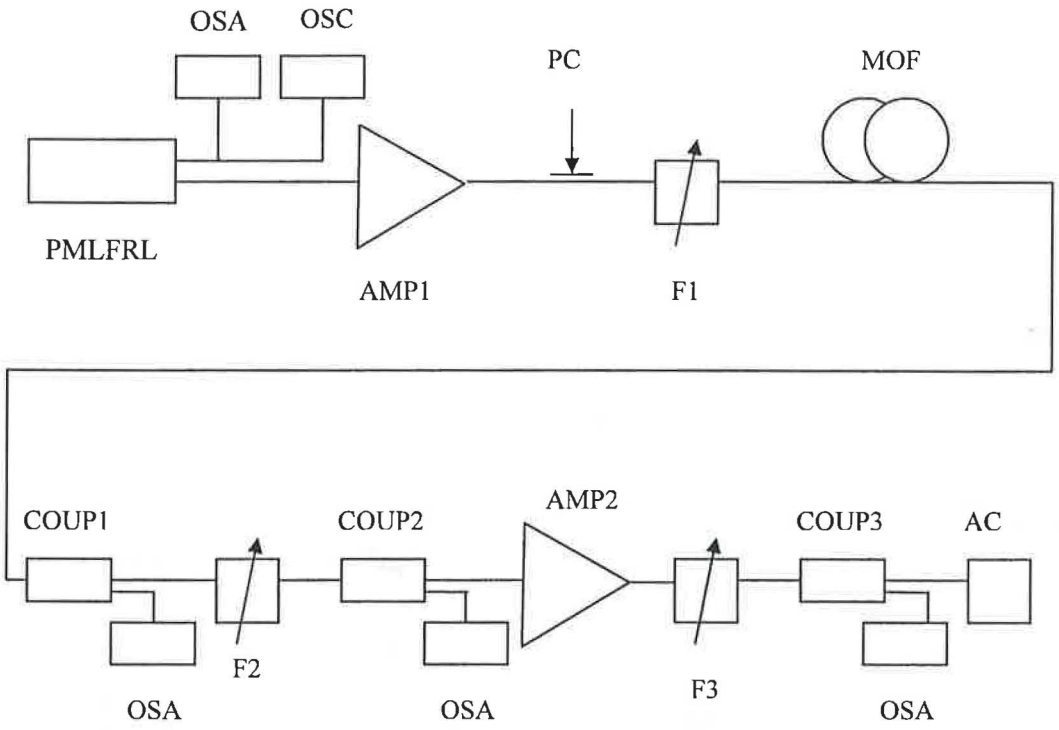

Fig. 5.3.1 Experimental setup. The inputs to the optical spectrum analyser OSA were switched by an optical switch (not drawn for clarity).

The pulses from the laser were amplified by the fibre amplifier AMP1 (company INO), which produced average output powers around 4.5 mW. The amplified spontaneous emission from the AMP1 was suppressed by a bandpass filter with a 3-nm full-width at half-maximum. A polarization controller (PC) was placed before the MOF due to fibre birefringence.

The supercontinuum generated in the MOF was observed at the OSA using a 90/10 coupler (COUP1). The spectral slicing of the supercontinuum was performed by a tunable filter (F2) with a 2.87-nm width at 3dB level. A 90/10 coupler (COUP2) was used to monitor the position of the filter F2 in the spectrum. The signal behind the filter F2 was too weak to detect it at an autocorrelator. Therefore, another fibre amplifier AMP2 was used to increase the signal. The filter F3 reduced the amplified spontaneous emission from the AMP2 and the output signal was led to the OSA and to the autocorrelator AC through the 99/1 coupler COUP3.

The spectrum from the fibre laser is shown in Fig. 5.3.2. The Kelly's sidebands of the first order are evident. The small peak near the central wavelength is an artifact of a continuous wave circulating in the laser due to unsufficient modulation. This peak can be suppressed by setting the polarization controler in the laser.

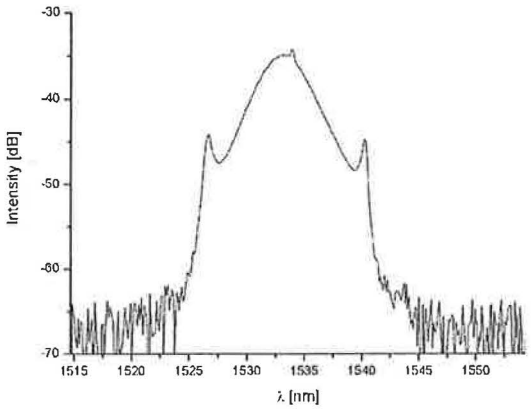

Fig. 5.3.2 Spectrum of a sub-picosecond soliton fibre laser.

The spectrum from the fibre laser, the generated SC in the MOF and the spectra behind the filters F2 and F3 are shown in Fig. 5.3.3.

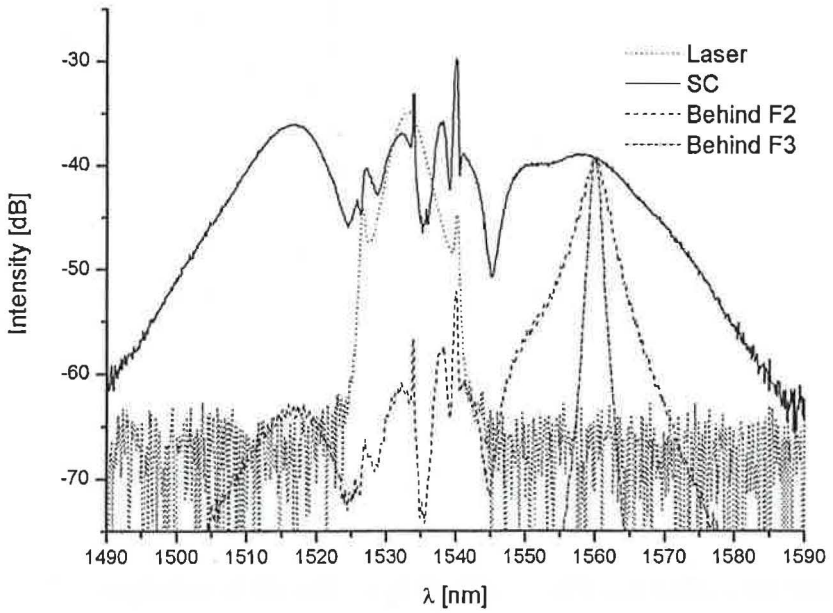

Fig. 5.3.3 Laser spectrum, supercontinuum from MOF and spectra behind F2 and F3.

It can be noticed that the small peak from the laser spectrum was also present in the generated supercontinuum. The best flatness of the SC generated in the MOF was in the range between 1550 nm and 1560 nm. Therefore, the filters F2 and F3 were tuned to 1560 nm to demonstrate the clock-signal conversion.
Then, we were trying to optimize the properties of the converted pulses at 1560 nm. The filter F3 was taken away and the autocorrelation traces of the converted pulses were measured for four levels of the AMP2 pumping (see Fig. 5.3.4).

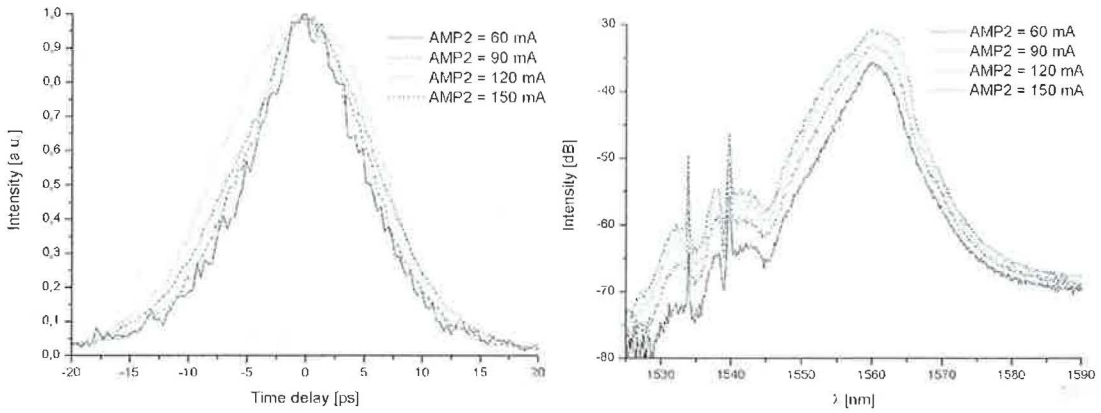

(a) (b)

Fig. 5.3.4 Autocorrelation traces (a) and spectra (b) of the amplified converted pulses for various levels of the AMP2 pumping.

With decreasing the pumping the AMP2, the signal-to-noise ratio decreases due to the amplified spontaneous emission (around 1540 nm) of the amplifier. A 150-mA level of the pumping was found to be ideal. The autocorrelation traces of the converted pulse with and without the filter F3 are shown in Fig. 5.3.5.

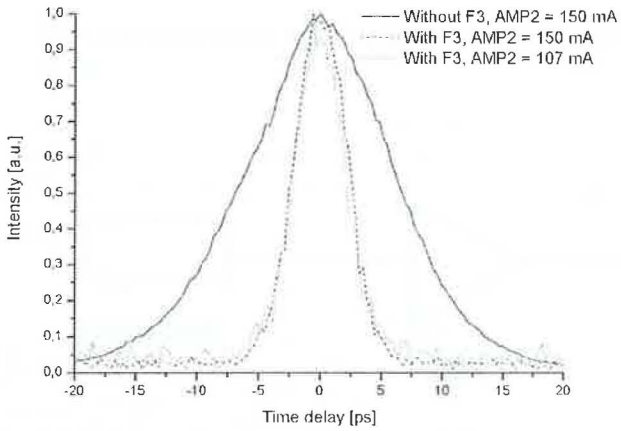

Fig. 5.3.5 Comparison of the autocorrelation traces with and without the filter F3.

The width and the signal-to-noise ratio of the converted pulses do not depend significantly on the pumping AMP2, if the filter F3 is used.

5.4 Supercontinuum generation in MOF and highly-nonlinear conventional fibres using a tunable picosecond laser TMLL-1550

5.4.1 Optimization of input pulses

The tunable passively mode-locked laser TMLL-1550 with a repetition rate of 10.3 GHz was used as a pulse source to demostrate the differences between properties of

supercontinua generated in the microstructured fibre (MOF) and in the highly-nonlinear conventional fibres (HNLF). The output spectrum of the laser tuned to 1524.2 nm and 1531 nm in linear and logaritmic scale are shown in Fig. 5.4.1.

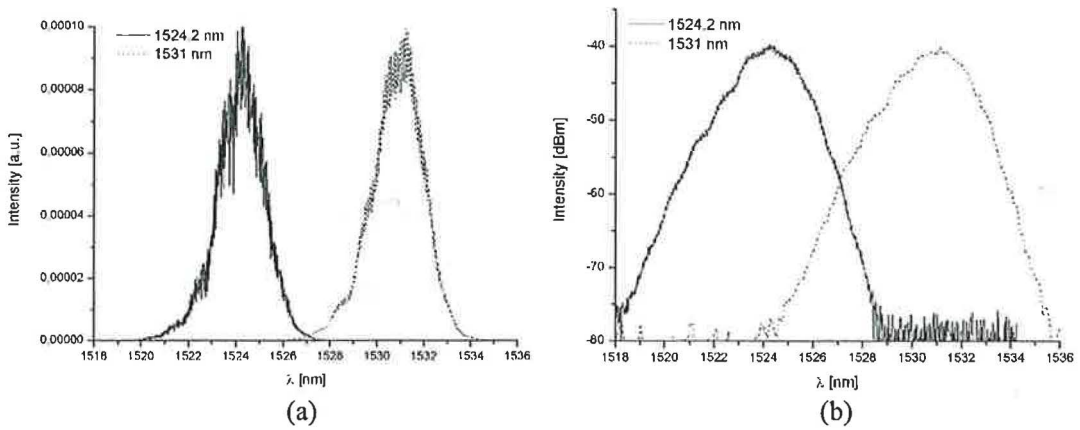

Fig. 5.4.1 The output spectra of the laser TMLL-1550 in (a) linear scale, (b) logaritmic scale. The spectra are modulated with the repetition rate of the laser (10.3 GHz). The pump current of the laser was 77 mA.

The autocorrelation of the pulses was not detectable. Therefore, the setup in Fig. 5.4.2 was used.

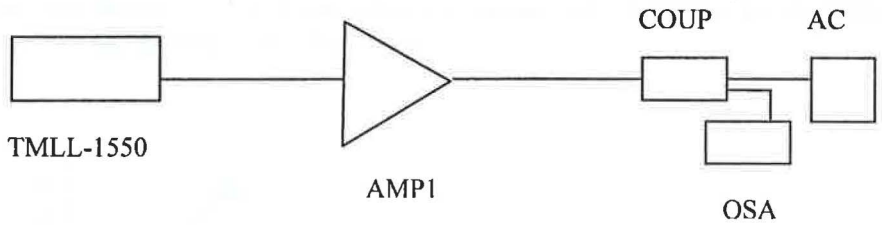

Fig. 5.4.2 Experimental setup for measuring the spectra and autocorrelation traces of the amplified pulses from the laser TMLL-1550.

The pulses from the laser TMLL-1550 at 1531 nm were amplified in the fibre amplifier AMP1 (Keopsys) with an output power up to 20 dBm. The output power of the AMP1 was set to 13.3 dBm. The coupler COUP with a coupling ratio 99/1 was placed at the AMP1 output in order to measure the output spectrum and autocorrelation traces of the pulses with the optical spectrum analyzer OSA and with the autocorrelator AC, respectively. The autocorrelation trace for a 77-mA laser pumping showed that two pulses were propagating simultaneously in the laser cavity. This feature indicated the soliton regime of the laser, when the fundamental soliton decayed into solitons of the higher order because of an excessive energy in the laser cavity (see Sec. 4.5). The laser pumping was decreased to 63.3 mA, when only one pulse was observable at the autocorrelation trace. The autocorrelation traces for the laser pumping 77 mA and 63.3 mA are plotted in Fig. 5.4.3a.

The spectrum after amplification is shown in Fig. 5.4.3b. There were no observable changes in the spectrum when the laser pumping decreased from 77 mA to 63.3 mA.

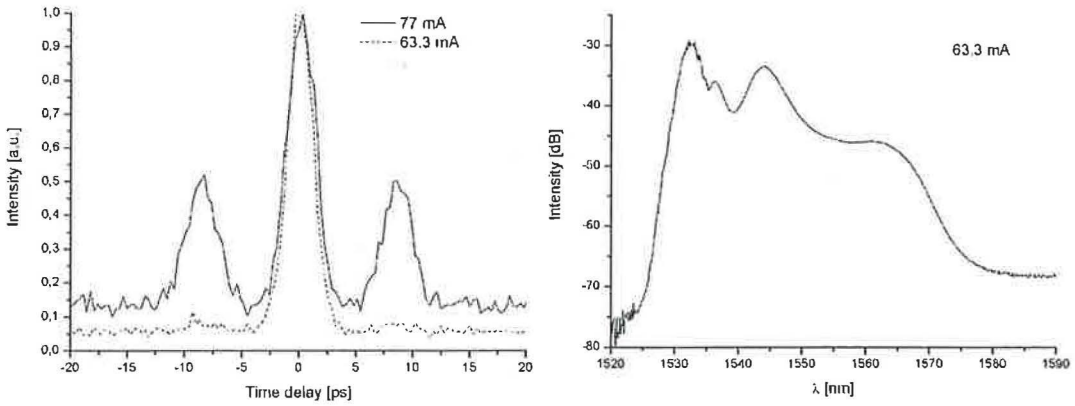

(a) (b)

Fig. 5.4.3 (a) The autocorrelation trace of the amplified pulses for the laser pumping 77 mA and 63.3 mA; (b) the spectrum for laser pumping 63.3 mA (the spectrum for 77 mA was nearly identical).

The increase of a long-wavelength part of the spectrum in Fig. 5.4.3b is caused by the amplified spontaneous emission (ASE) in the amplifier. In the autocorrelation traces in Fig. 5.4.3a, the ASE appears as an incoherent pedestal. It is necessary to suppress the influence of the ASE in order to improve the coherent properties of the generated SC. Furthermore, the ASE would affect the long-wavelength part of the SC. Therefore, the laser was tuned to 1538.9 nm, when the largest ratio between the laser peak and the ASE occurs in the spectrum (see Fig. 5.4.4).

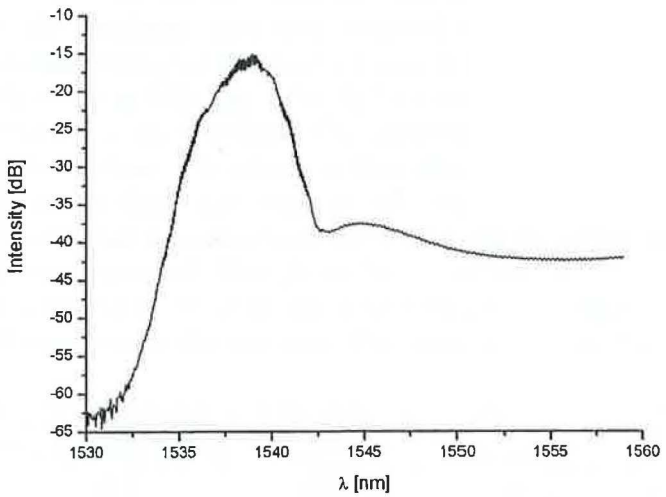

Fig. 5.4.4 The spectrum for the laser pumping 63.3 mA after tuning to 1538.9 nm. The laser peak to the ASE ratio improved to about 20 dB.

5.4.2 Experimental setup

The experimental setup for the SC generation is shown in Fig. 5.4.5.

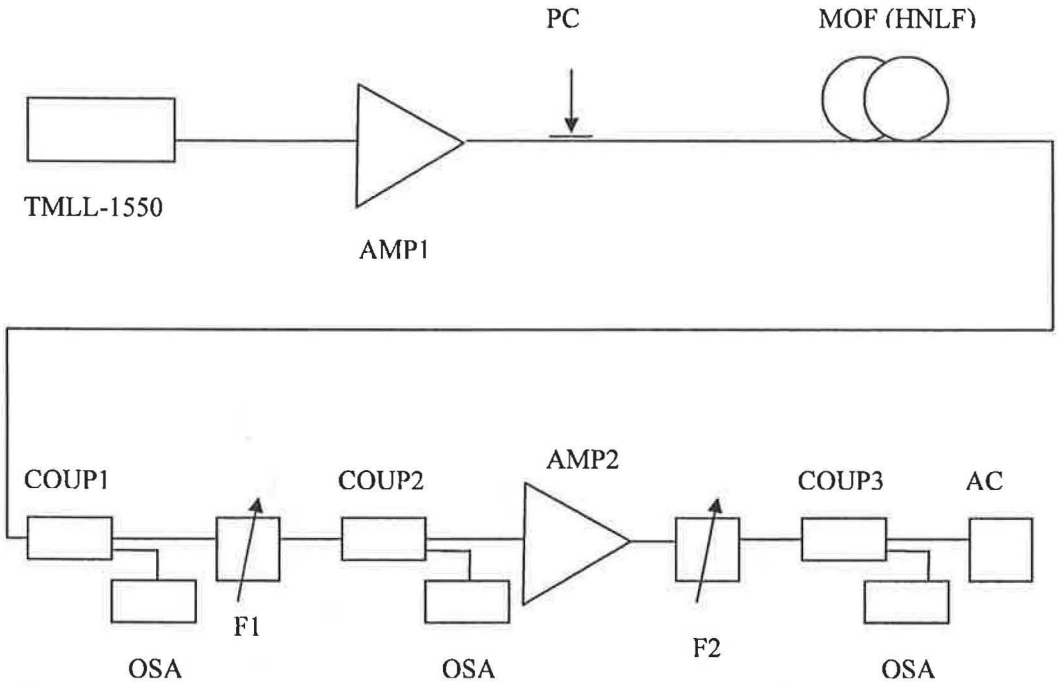

Fig. 5.4.5 Experimental setup for the SC generation. The inputs to the optical spectrum analyser OSA were switched by the optical switch (not drawn for clarity).

The central wavelength of the laser TMLL-1550 was set to 1538.9 nm, the pump current of the laser was 63.3 mA. The pulses from the laser were amplified by the fibre amplifier AMP1 (Keopsys) with an output power up to 20 dBm. The polarization controller PC was placed before the nonlinear fibre due to fibre birefringence. The supercontinuum generated in the nonlinear fibre was observed at the OSA using the 90/10 coupler COUP1. The spectral slicing of the supercontinuum was performed by the tunable filter F1 with a 2.87-nm width at 3dB level. The 90/10 coupler COUP2 was used to monitor the position of the filter F1 in the spectrum. The signal behind the filter F1 was too weak to detect it at the autocorrelator. Therefore, another fibre amplifier AMP2 (Keopsys) with an output power up to 10 dBm was used to increase the signal. The filter F2 reduced the amplified spontaneous emission from the AMP2 and the output signal was led to the OSA and to the autocorrelator AC through the 99/1 coupler COUP3.
The output power from the AMP1 varied in a range 13 dBm – 21.5 dBm. The parameters of the pulses at the nonlinear fibre input are in Tab. 5.4.1.

Tab. 5.4.1 Parameters of the pulses at the nonlinear fibre input.

P_{out} (AMP1) [dBm]	P_{avg} [mW]	T_{FWHM} [ps]	P_0 [W]	$\Delta\lambda_{FWHM}$ [nm]	C
13.0	16.8	1.64	0.93	2.8	0.87
15.3	29.4	1.51	1.8	2.9	0.76
18.0	56.2	1.59	3.2	3.1	0.98
20.0	86.3	1.85	4.3	3.2	1.4
21.5	128.8	1.89	6.2	3.3	1.5

P_{avg} denotes the average power at the nonlinear fibre input. The chirp parameter C was calculated from the relation

$$\Delta T_{FWHM} \cdot \Delta \omega_{FWHM} = 4\sqrt{1+C^2}\ln 2, \tag{5.4.1}$$

assuming the Gaussian pulse shape.

5.4.3 Supercontinuum generation in the microstructured fibre

The spectrum of the pulse did not broaden significantly in a 10-m MOF. The spectrum measured with the OSA behind the COUP2 for the highest output power from the AMP1 (see Fig. 5.4.5) is plotted in Fig. 5.4.6.

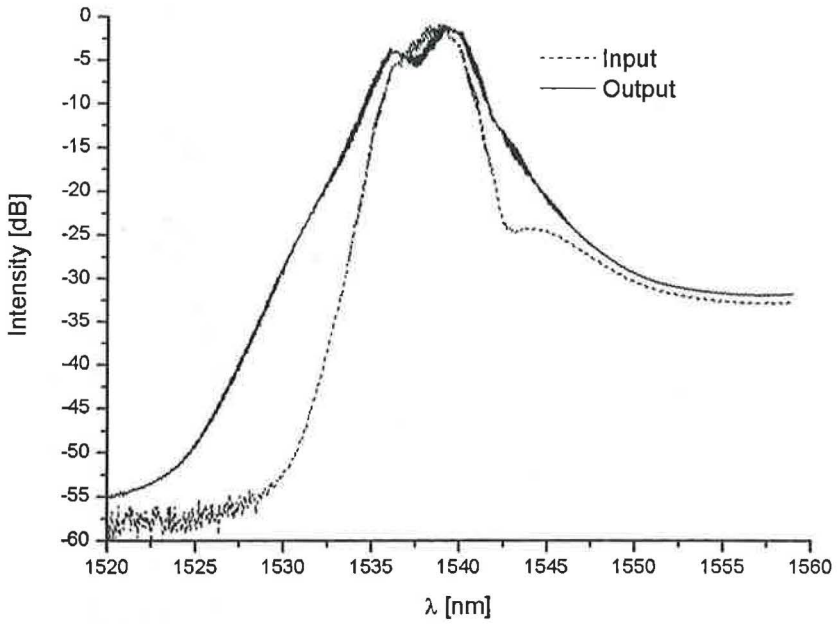

Fig. 5.4.6 Input and output spectrum for a pumping AMP1 of 21.5 dBm.

The 10.3-GHz modulation of the laser spectrum is observable in the output spectrum, too. The conversion of the pulses to other wavelength could not be demostrated because of a small width of the generated spectrum.
Numerical simulations were performed in order to investigate the SC generation in the MOF at higher peak powers of the input pulses. First, the SC generation for the peak power of 6.2 W was simulated for comparison with the experimental results. Fig. 5.4.7 shows the simulated spectrum for the peak power 6.2 W, which corresponds to the experimental conditions.

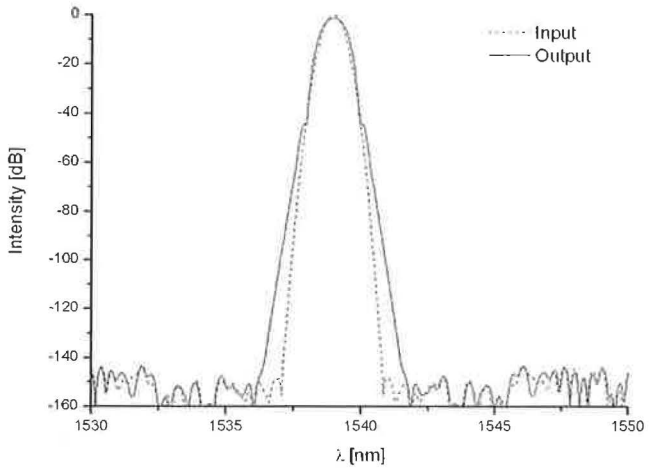

Fig. 5.4.7 Simulated spectra from the MOF for the peak power 6.2 W.

A simulated spectral broadening is very small, in accordance with the experimental results. Further simulations for higher initial peak powers (100 W, 200 W, 300 W and 400 W) were carried out. The simulated output spectra from the MOF are plotted in Fig. 5.4.8.

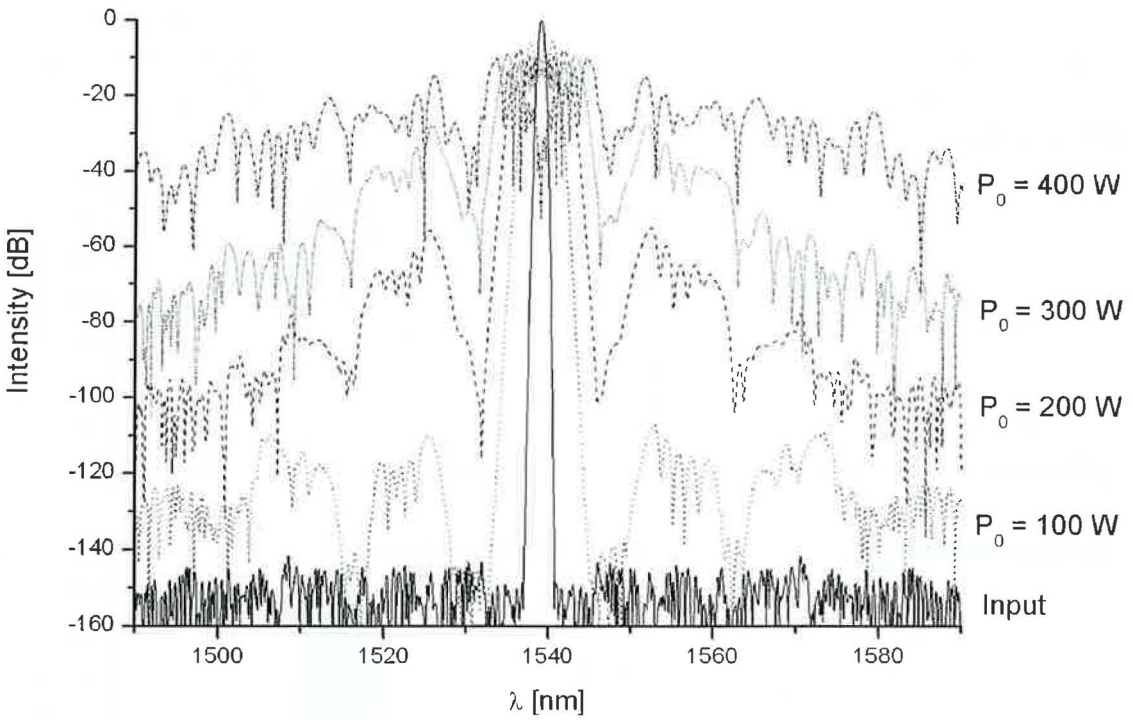

Fig. 5.4.8 Simulated supercontinua from the MOF for initial peak powers 100 W, 200 W, 300 W and 400 W.

The spectra broaden symmetrically due to self-phase modulation. Peak powers around 400 W were required for a sufficient signal in the range 1550 -1560 nm.
Simulated output pulse shapes and autocorrelation traces for these peak powers are shown in Fig. 5.4.9.

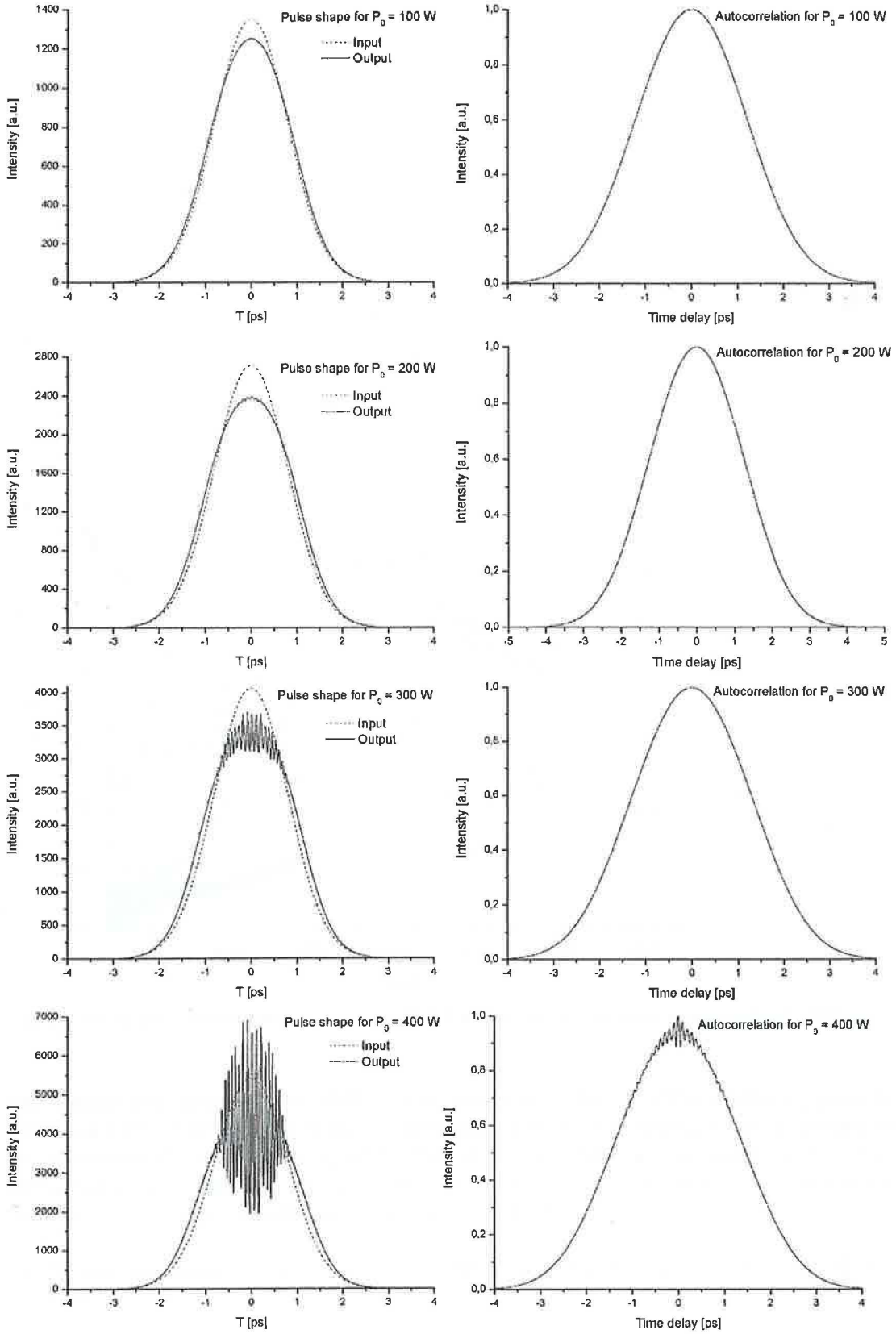

Fig. 5.4.9 Simulated pulse shapes (left column) and autocorrelation traces (right column) of the pulses at the output the MOF for initial peak powers 100 W, 200 W, 300 W and 400 W.

A significant modulation of the pulse shape for $P_0 = 400$ W is evident. This modulation leaded to the spectral broadening. The pulses did not exhibit decay. Therefore, the spectral slicing of the spectra could be performed in order to get a converted clock signal.

5.4.4 Supercontinuum generation in a 1.01-km HNLF with a zero-dispersion wavelength of 1560 nm

The microstructured fibre was replaced by the highly-nonlinear conventional fibre (HNLF) with a length of 1010 m and a zero-dispersion wavelength of 1560 nm. The pump wavelength 1538.9 nm fell into the normal-dispersion regime of the fibre. It is worth noticing that a part of the SC was generated in the anomalous-dispersion regime, which involves soliton effects during SC generation. The output spectra from the HNLF are shown in Fig. 5.4.10 for the AMP1 output power as a parameter.

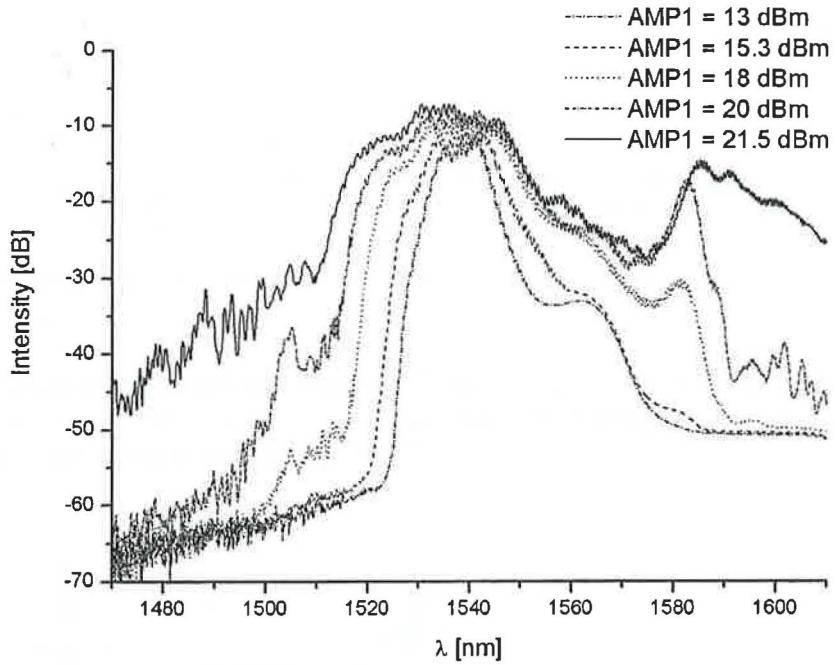

Fig. 5.4.10 Spectra generated in a 1.01-km HNLF with a zero-dispersion wavelength of 1560 nm.

The spectra generated with the AMP1 output power more than 18 dBm exhibit depletion in the range 1550-1580 nm. The Stokes components of four-wave mixing were observable in the anomalous-dispersion region, while blue-shifted anti-Stokes components appeared in the region around 1500 nm. Those spectra can not be used for the clock-signal conversion because of more than a 10-dB depletion around 1560 nm.

5.4.5 Supercontinuum generation in a 500-m HNLF with a zero-dispersion wavelength of 1529 nm

In order to demonstrate the SC generation in the anomalous-dispersion regime, a 500-m highly-nonlinear conventional fibre with the zero-dispersion wavelength at 1529 nm was used. The generated spectra are plotted in Fig. 5.4.11.

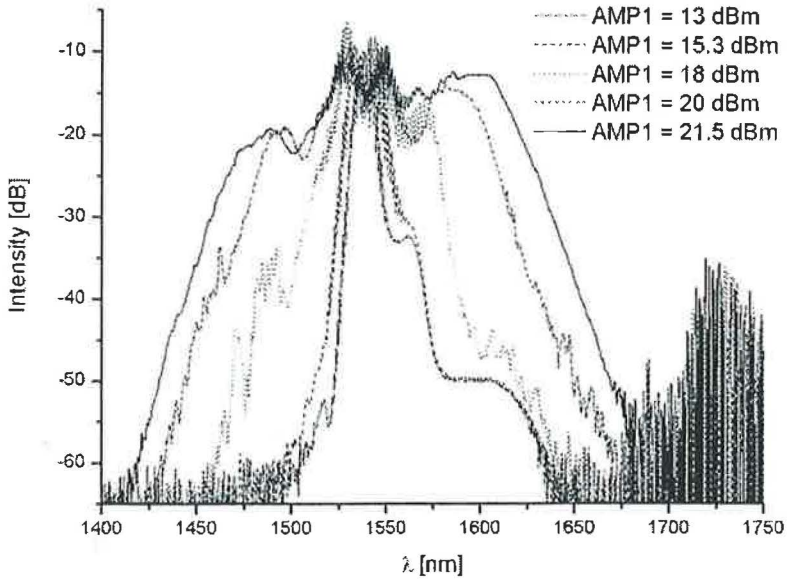

Fig. 5.4.11 Spectra generated in a 500-m HNLF with a zero-dispersion wavelength of 1529 nm.

The generated supercontinua are affected by an energy transfer into a long-wavelength part of the spectrum, a typical feature of the SC generation in long fibres. The flatness is not sufficient for applications like the clock-signal conversion.

5.4.6 Supercontinuum generation in a 500-m HNLF with a zero-dispersion wavelength of 1543 nm

The greatest bandwidth and flatness of the SC were achieved with a 500-m highly nonlinear conventional fibre with a zero-dispersion wavelength of 1543 nm. The generated supercontinua are plotted in Fig. 5.4.12.

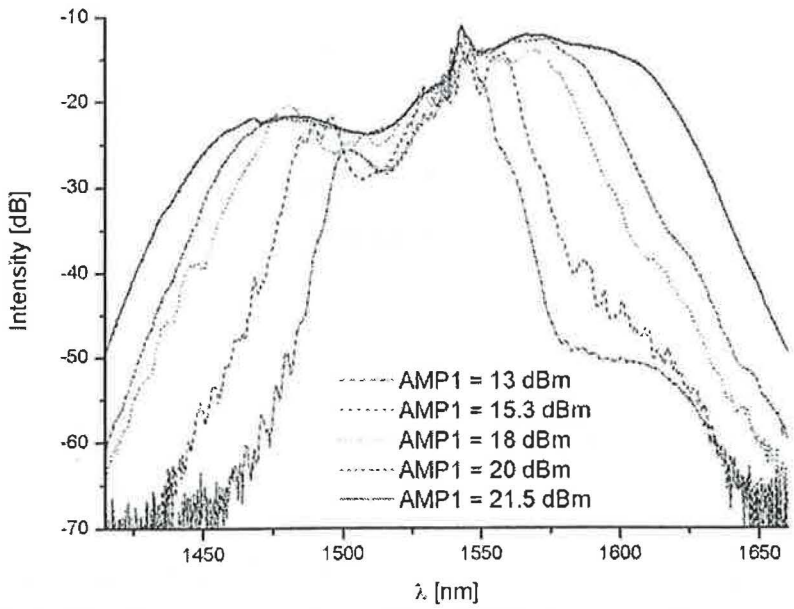

Fig. 5.4.12 Spectra generated in a 500-m HNLF with a zero-dispersion wavelength of 1543 nm.

The supercontinua generated in this nonlinear fibre exhibited a great bandwith and flatness, especially in the range 1550-1600 nm. The spectral slicing at 1560 nm was performed to demonstrate the clock signal conversion. The spectra behind the filters F1 and F2 are shown in Fig. 5.4.13.

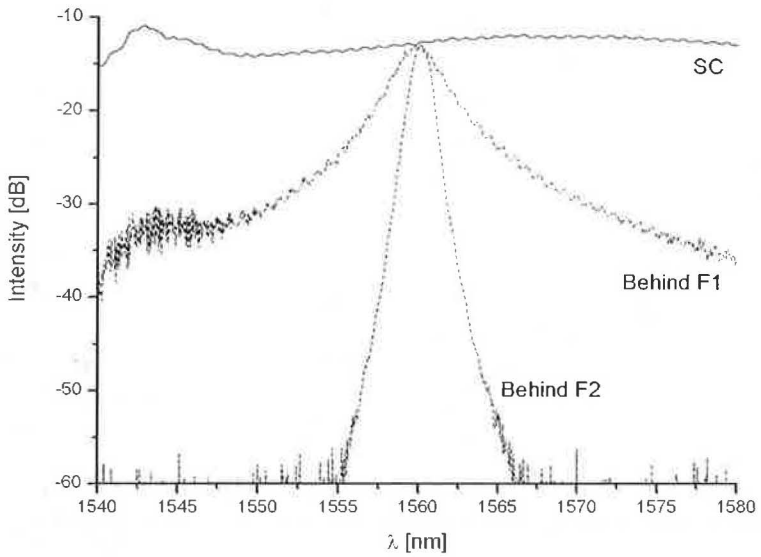

Fig. 5.4.13 Supercontinuum and spectra behind the filters F1 and F2 (the output power of the AMP1 was 21.5 dBm).

However, no pulses were detected at the autocorrelator. It could be explained by decay of the pulses. Numerical simulations were performed in order to illustrate the pulse evolution during the propagation in the fibre (see Fig. 5.4.14). The parameters of the initial pulse were taken from Tab. 5.4.1 for the case of the AMP1 output power 21.5 dBm.

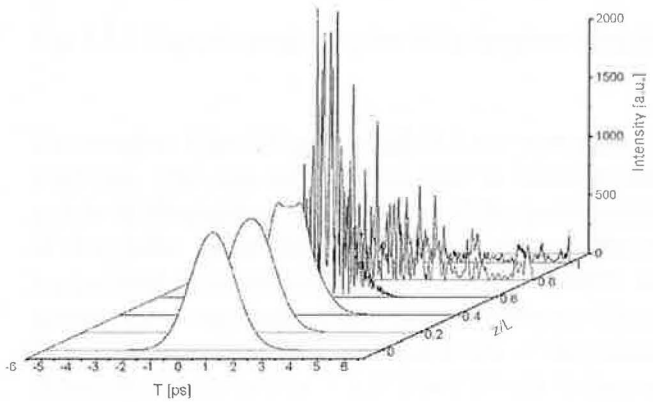

Fig. 5.4.14 Simulation of the pulse evolution in a 500-m HNLF with a zero-dispersion wavelegth of 1543 nm.

The numerical simulation shows that the pulse undergoes decay. That is why the autocorrelation was not detectable.

5.5 SC generation in three HNLFs

Three highly-nonlinear fibres - a 1010-m HNLF with a zero-dispersion wavelength of 1560 nm, a 500-m HNLF with a zero-dispersion wavelength of 1560 nm and a 500-m HNLF with a zero-dispersion wavelength of 1529 nm were connected. The laser TMLL-1550 central wavelength was set to 1538.6 nm. The experimental setup is shown in Fig. 5.5.1.

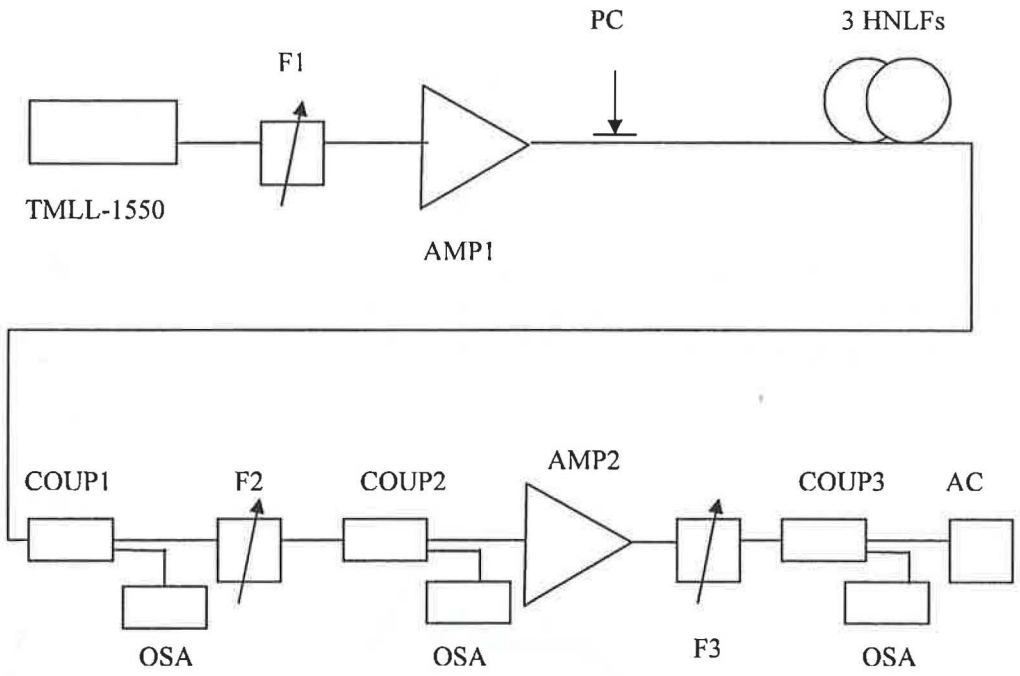

Fig. 5.5.1 Experimental setup for SC generation using three connected nonlinear fibres.

The tunable filter F1 of a width 0.5 nm was placed at the laser output and tuned to around 1538 nm. The role of the filter was to increase the pulse width and to decrease the peak power of the pulses. The decrease of the peak power was caused by filtering out outer parts of the pulse spectrum. Due to this, undesirable nonlinear effects in the amplifier were suppressed. The output power from the AMP1 was 20 dBm. The decrease in the peak power was compensated by a longer nonlinear fibre.
The autocorrelation trace and spectrum of the pulses launched into the connected nonlinear fibres are shown in Fig. 5.5.2. The FWHM of the pulses was about 9 ps.

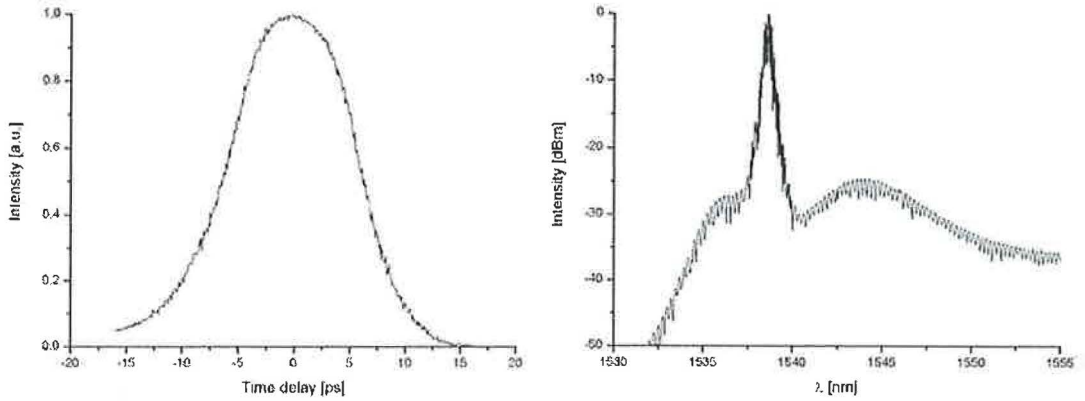

Fig. 5.5.2 The autocorrelation trace (a) and the spectrum (b) of filtered pulses behind the polarization controller PC (see Fig. 5.5.1).

The spectrum behind three connected nonlinear fibres is plotted in Fig. 5.5.3. It exhibits a great flatness in the C-band used for optical communication (1530 nm – 1565 nm). However, the spectrum descended significantly in this range, when the output power from the AMP1 decreased slightly.

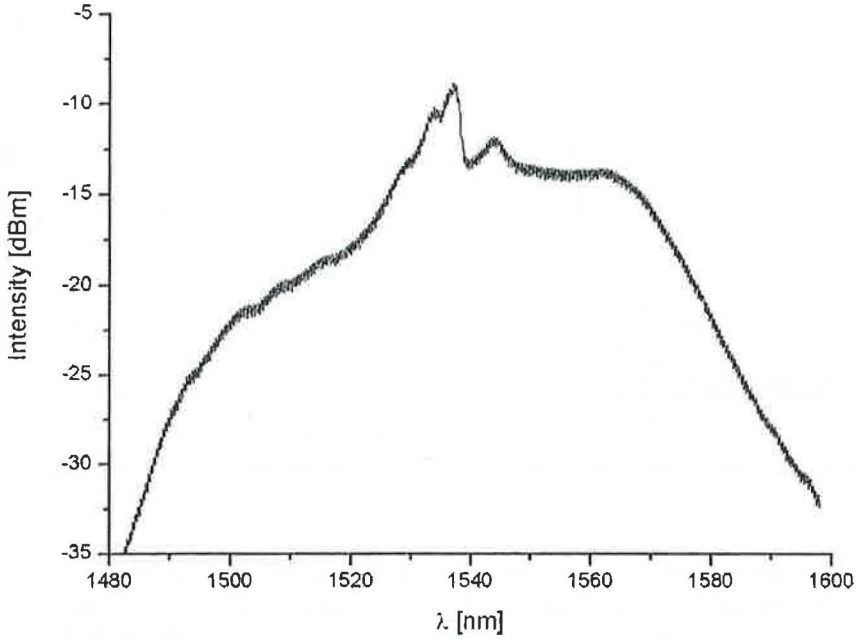

Fig. 5.5.3 Supercontinuum generated in three connected nonlinear conventional fibres.

The spectral slicing of the SC was performed to demonstrate the clock-signal conversion. The filters F2 and F3 were tuned to 1541.9 nm, 1550.0 nm and 1560.1 nm. The autocorrelation traces behind the F3 and spectra behind the F2 and the F3 are shown in Fig. 5.5.4.

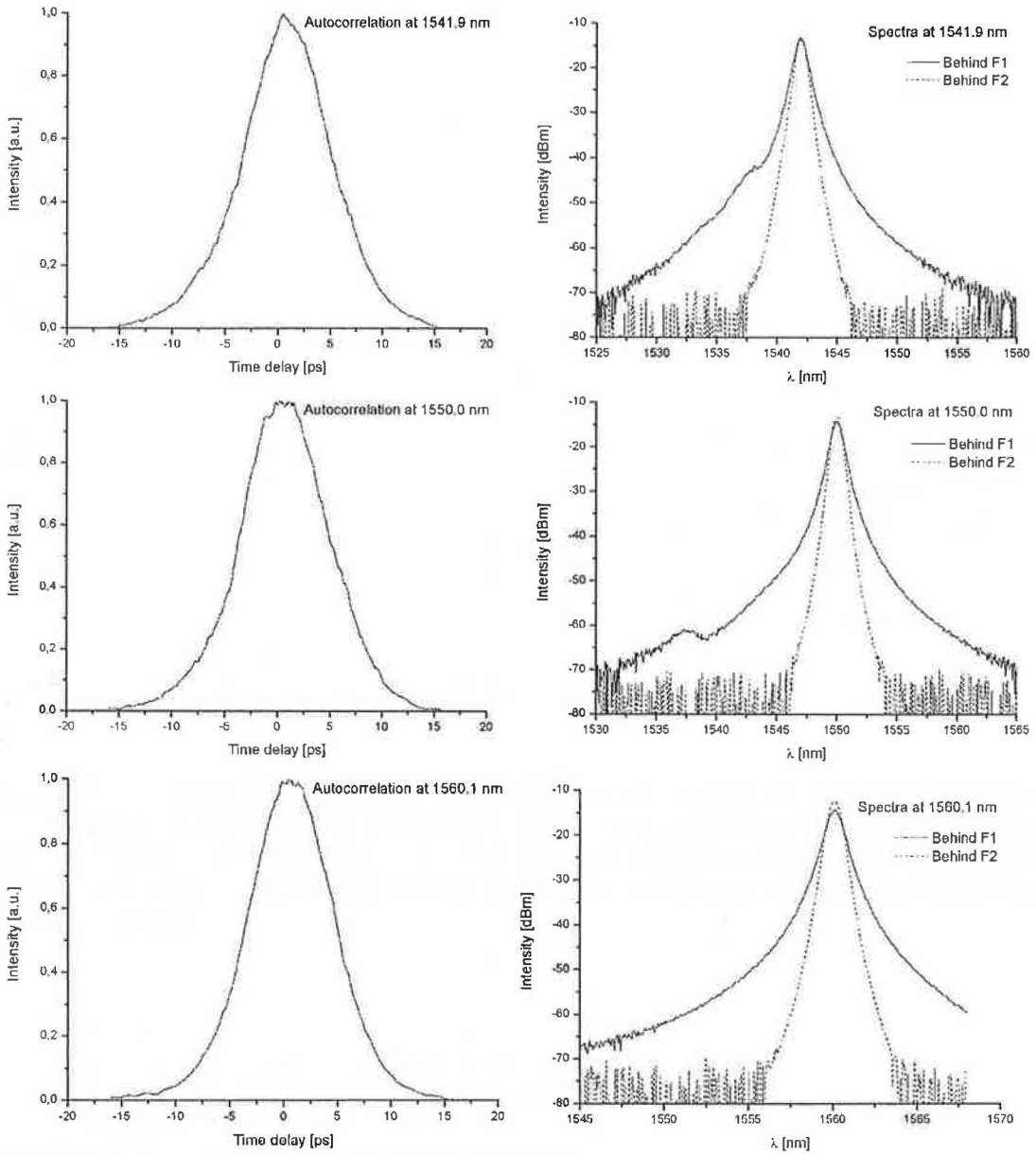

Fig. 5.5.4 Autocorrelation traces and spectra at 1541.9 nm, 1550.0 nm and 1560.1 nm.

The experimental realization of the SC source for wavelength division multiplexing (WDM) systems was also demonstrated. The output power of the AMP1 was increased to 21.5 dBm (the shape of the generated SC remained unchanged). The filter F2 from the Fig. 5.5.1 was replaced by the multiplexor and demultiplexor. The experimental setup is shown in Fig. 5.5.5.

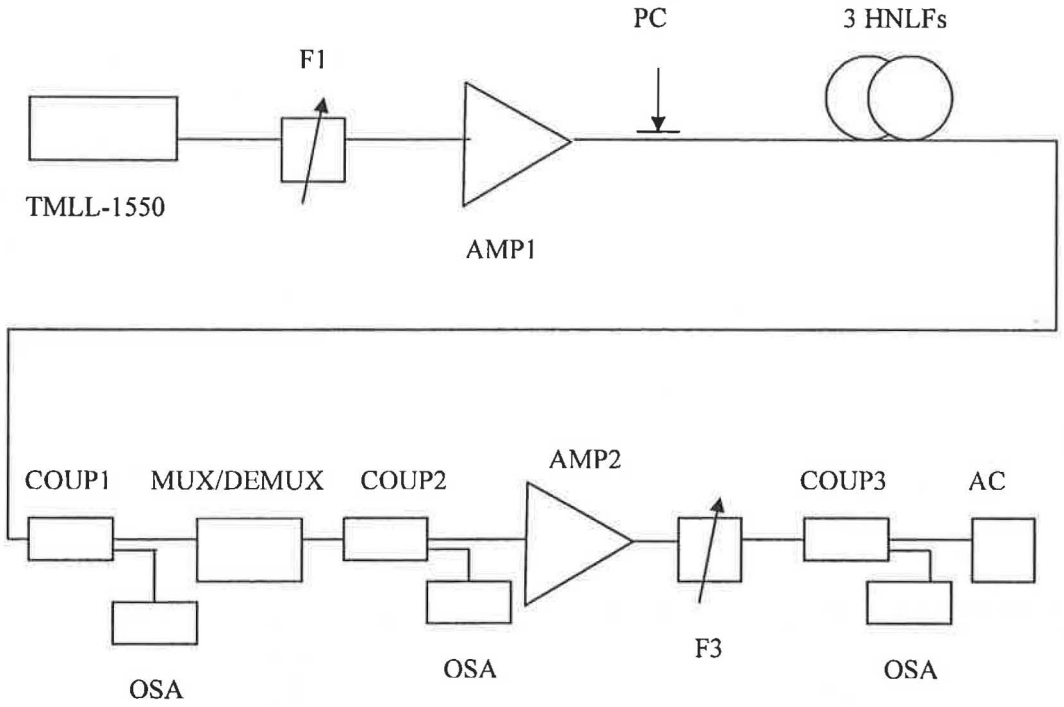

Fig. 5.5.5 Experimental setup for a demonstration of a WDM source.

The multiplexor and demultiplexor were coupled in order to observe all spectral channels. Finally, the demultiplexor was taken away and one selected channel was detected at the OSA and at the AC. Fig. 5.5.6 shows the spectrum after the coupled multiplexor and demultiplexor, and the spectrum in one channel of the multiplexor, when the demultiplexor was disconnected.

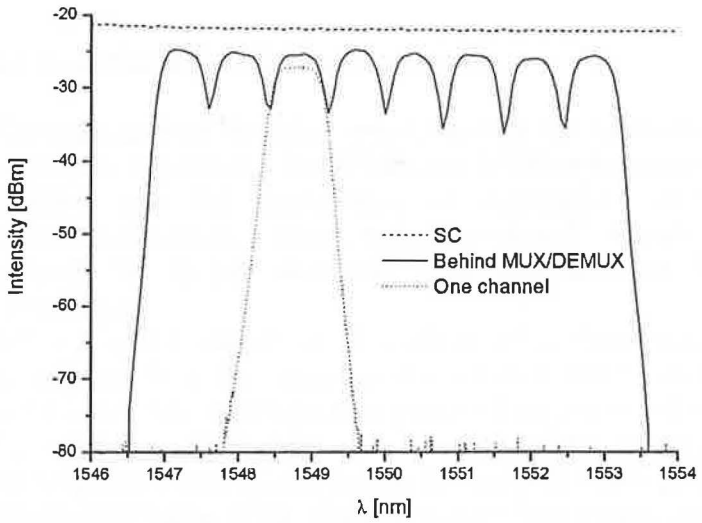

Fig. 5.5.6 Supercontinuum, the spectrum behind the MUX/DEMUX and the spectrum in one channel of the multiplexor.

Uniform intensities in all spectral channels were achieved. However, the real application would require an actively-mode locked laser that ensures an exactly defined repetition rate of pulses.
The signal from the one channel of the multiplexor was amplified by the AMP2 (an output power of 12.3 dBm) in order to detect the autocorrelation trace. The filter F3 was used to eliminate the amplified spontaneous emission from the AMP2. The spectrum behind the F3 and the autocorrelation trace of the pulses in the channel is plotted in Fig. 5.5.7.

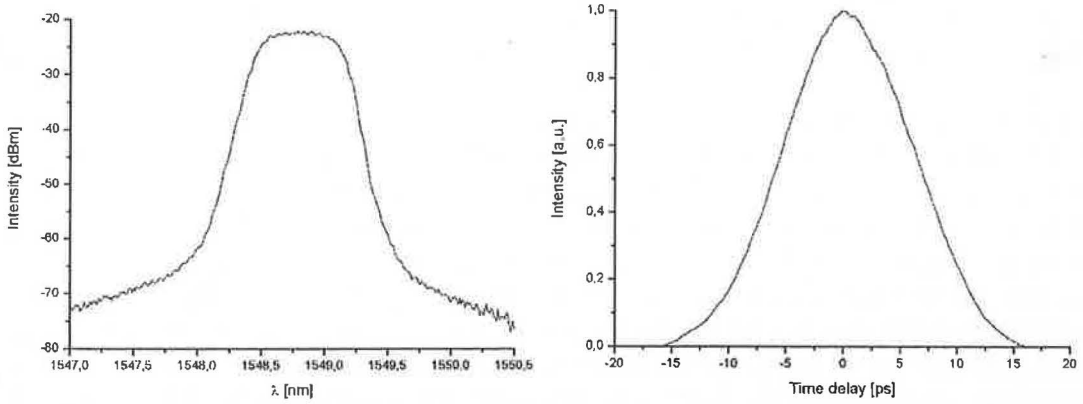

(a) (b)

Fig. 5.5.7 Measurement of one selected channel of the multiplexor. (a) The spectrum after amplification behind the F3; (b) the autocorrelation trace of the pulses.

Similar spectra and autocorrelation traces would be measured in other spectral channels, too.

6. Conclusion

6.1 Experimental and numerical results

The main goal of the thesis was optimizing the supercontinuum (SC) characteristics with respect to applications in OTDM and WDM telecommunication systems. This task was fulfilled and the possibilities of applications of SC in OTDM and WDM telecommunications systems were demostrated. A variety of input pulses was used to generate SC in four nonlinear fibres with different lengths and the zero-dispersion wavelengths.
Sec. 5.2 brings numerical simulations of a time evolution of the pulse when it is propagating in a 10-m microstructured fibre (MOF) used in experiments. The simulations were performed for a high peak power of the pulse and a small pulse width ($P_0 = 640$ W, $T_0 = 0.244$ fs). Dependence of the SC generation on a chirp of initial pulses was investigated. It was shown that the SC bandwidth (at a given intensity level) increases with the absolute value of the chirp parameter. The bandwidth of the generated SC was larger for the case of the negative initial chirp. Detrimetal decay of the pulses after propagating a half of the fibre length was found. Therefore, a shorter fibre or lower peak powers should

be used in experiments in order to get an autocorrelation trace correnspondingto non-decayed output pulses. According to (4.4.9), shortening of the fibre is equivalent to decreasing the peak power.

In Sec. 5.3, the SC generation in the 10-m MOF was demonstrated using sub-picosecond pulses from a passively mode-locked fibre laser working in the soliton regime. Peak powers were lower than those in the simulations from Sec. 5.2. A great flatness of the generated SC was achieved in the range 1550 nm – 1560 nm, which is important for telecommunication applications. A tunable optical clock translator for OTDM systems was demonstrated using the spectral slicing of the supercontinuum at 1560 nm. The converted pulses were amplified in order to measure their autocorrelation traces at the autocorrelator. The spectrum after amplification was filtered to suppress the negative influence of the ASE from the amplifier.

Longer pulses (more than 1 ps) with lower peak powers were used to generate SC in the MOF and in three highly nonlinear convential fibres (HNLFs), as described in Sec. 5.4. A great significance was assigned to the optimization of pulses launched into the nonlinear fibres. Methods of the optimization were described in Sec. 5.4 (setting a laser regime, suppression of the ASE from the amplifier). The 10-m MOF was found to have an insufficient length for the SC generation with picosecond pulses, because the spectral broadening was not significant. According to the relation (4.4.9), the unsufficient length of the fibre can be compensated by increasing the peak power of the pulse. This increasing was not possible in our experiment. Therefore, numerical simulations were performed instead.

First, a simulation of the output spectrum from the MOF for the case of the peak power 6.2 W was performed for comparison with the experimental results. The simulated output spectrum from the MOF (Fig. 5.4.7) corresponds qualitatively to the measured spectrum (Fig. 5.4.6). The output spectra are similar and the simulated spectral broadening is in accordance with the experimental results. The numerical model did not include the amplified spontaneous emission produced by the amplifier (a long-wavelength part of the spectrum). The spectral width in the simulation is smaller in comparison with the experiment. However, the simulated spectral width is critically dependend on a choice of the pulse shape (which could not be determined experimentally). Therefore, the Gaussian shape used in simulations was only an approximation of a real pulse shape. The simulations for higher peak powers show that the spectrum broaden significantly for peak powers exceeding 300 W, while the peak power in the experiment was 6.2 W. The spectra broaden symmetrically, what is a typical feature of SC generation in the normal-dispersion regime. Further simulations were performed in order to simulate the pulse shape at the output from the MOF. The simulations indicate that the propagating pulse does not exhibit decay. Therefore, coherence in the simulated supercontinua would be sufficient for a spectral slicing and detection of converted pulses at the autocorrelator.

Experiments with the highly-nonlinear conventional fibres instead of the MOF showed differences in the output spectra in dependence of the relative position of the pump wavelength and the zero-dispersion wavelength of a nonlinear fibre. The lengths of the conventional fibres (500 m and 1010 m) were sufficient for a significant spectral broadening. The spectra generated in a 1010-m long HNLF with a zero-dispersion wavelength of 1560 nm exhibited depletion in the range 1550 – 1580 nm. Therefore, they were not suitable for telecommunication applications. This depletion was caused by a high efficiency of four-wave mixing in a vicinity of the zero-dispersion wavelength [12]. The Stokes components appeared in the long-wavelength part of the spectrum, the anti-Stokes components were observable around 1500 nm.

The spectra generated in the anomalous-dispersion regime (in a 500-m HNLF with a zero-dispersion wavelength of 1529 nm) did not have flatness suitable for applications. The energy transfer to a red side of the spectrum was caused by the soliton self-frequency shift described by (4.2.28) in the anomalous-dispersion regime. Therefore, the SC generation in the normal-dispersion regime is more suitable, because the spectrum broadens nearly symmetrically.
The SC generation with the pump wavelength near the zero-dispersion wavelength was demonstrated using a 500-m HNLF with a zero-dispersion wavelength of 1543 nm. The generated spectra exhibited the energy transfer to longer wavelengths due to the soliton self-frequency shift in an anomalous-dispersion part of the spectrum. A great flatness of the spectrum in the range 1550-1560 nm was suitable for applications. However, no pulses were detected at the autocorrelation trace. This was explained by a numerical simulation of the evolution of the pulse shape. The decay of the pulse caused that no autocorrelation signal corresponding to regular pulses was detectable.
In Sec. 5.5, the pulses from the laser TMLL-1550 were broadened by the spectral filter to about 9 ps. A decrease of the peak power of input pulses was compensated by an increasing the length of a nonlinear fibre (three HNLFs were connected). The generated SC had the best obtainable properties, especially a great flatness in the telecommunication C-band (1530 nm – 1565 nm). The optical clock translation was demonstrated at 1540, 1550 and 1560 nm. The flatness and good coherence of the SC allowed a demonstration of a WDM source using a multiplexor. A real application of SC as a WDM source requires an actively-mode locked laser with a defined repetition rate. It was not available for our experiments. However, the optimization of pulses launched into the nonlinear fibre is critically important for supercontinuum applications.

6.2 Experimental issues of supercontinuum generation

Amplification of short (sub-picosecond) pulses was found to be a significant problem in the SC generation. Nonlinear effects during the amplification can lead even to decay of the pulse. Most of erbium-doped fibre amplifiers have a fibre with a small field area, which causes the detrimental nonlinear effects during the amplification. One possibility is to use an amplifier with a large field area, which considerably reduces nonlinear effects. Another way (presented in our experiments with the TMLL-1550 laser) is to broaden the time shape of the pulse before the amplification (using spectral filter, which decrease the spectral bandwidth of the pulse). The peak power of the pulse descends because a part of the pulse spectrum is filtered out. Under specific conditions in the amplifier (a proper combination of gain, normal dispersion and nonlinearity) the similaritons can be generated. When the pulse is chirped, it can be compressed after aplification.
It is necessary to eliminate undesirable influences on the SC shape, especially an effect of the amplified spontaneous emission (ASE) from the amplifier. The ASE leads to the lost of coherence in the SC. Therefore, the spectrum of the pulse launched into the nonlinear fibre must be monitored. Further, a peak of a continuous wave in the laser spectrum can appear in the generated SC. This continuous wave is a consequence of an unsufficient modulation in the laser cavity. Fig. 6.2.1 shows how the ASE and the laser continuous-wave peak can affect the shape of generated SC.
The continuous-wave laser peak can be removed by proper setting mode-locking of the laser. The ways how to suppress of the ASE from the amplifier are presented in Secs. 5.3 and 5.4. One possibility is a use of the filter at the amplifier output. In the case of a tunable laser, the central wavelength of the laser can be tuned to the maximum of the ASE.

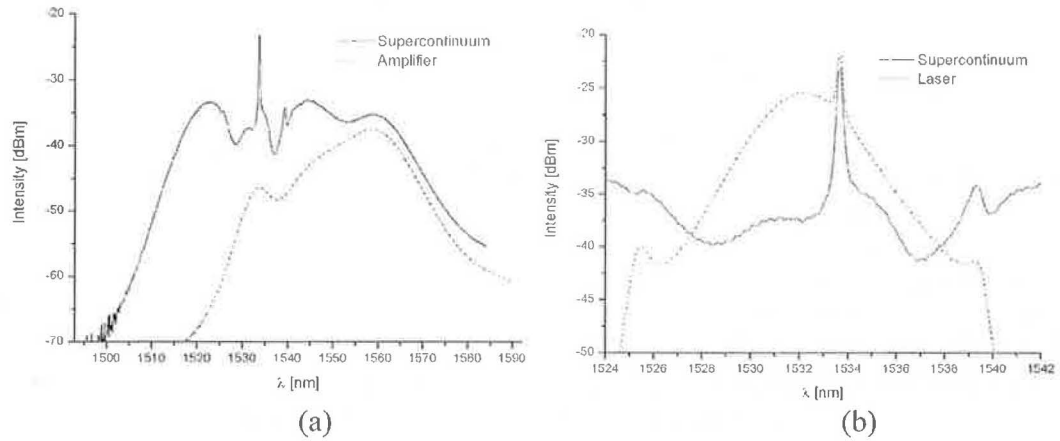

(a) (b)

Fig. 6.2.1 Negative influences on the shape of the generated SC. (a) ASE of the amplifier (with the laser switched off) and the generated SC. A long-wavelength part of the SC is strongly affected by the ASE, which causes the peak at 1560 nm. (b) Continuous-wave peak in the laser spectrum displayed in the generated SC around 1534 nm.

The MOF used in our experiment had significant birefringence. Therefore, the shape of the generated supercontinuum was dependent on the polarization of the input pulse. It was not observed in the long nonlinear fibres, because at long distances the initial polarization state of the pulse was not preserved.

The length of the standard-fibre pigtails of optical components and devices must be taken into an account, especially in the case of short and/or highly chirped pulses. The propagation of the pulse in a 1-m long pigtail between the amplifier output and the input to the MOF was simulated numerically. The pigtail was made from the standard single-mode anomalous-dispersion fibre SMF-28 with second-order dispersion $\beta_2 = -20\ \mathrm{ps^2 \cdot km^{-1}}$ at 1550 nm, third-order dispersion $\beta_3 = 0.17\ \mathrm{ps^3 \cdot km^{-1}}$ and the nonlinear coefficient $\gamma = 1.8\ (\mathrm{W \cdot km})^{-1}$. The simulation were performed for pulses from Tab. 5.4.1 for the case of output power from AMP1 equal to 21.5 dBm (T_{FWHM} = 1.89 ps, $P_0 = 6.2$ W). The simulated pulse shapes for chirp parameters $C = 1.5$ and 10 are plotted in Fig. 6.2.2.

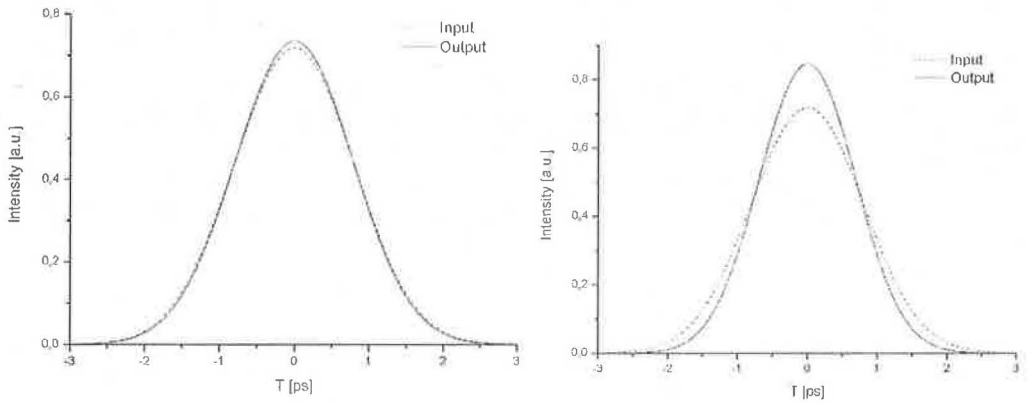

(a) (b)

Fig. 6.2.2 Simulation of the pulse propagation in a 1-m long pigtail from SMF-28 for initial chirps $C = 1.5$ (a) and $C = 10$ (b).

A value $C = 1.5$ corresponds to experimental conditions. Fig. 6.2.2 shows no significant changes of a peak power or pulse width for this value of a chirp parameter. However, in the case of $C = 10$ the pulse is compressed due to a compensation of an initial positive chirp in the anomalous-dispersion fibre, and its peak power increases significantly. Hence, the length of pigtails is important for high chirps of the pulse.
In order to detect an autocorrelation trace of converted pulses after a spectral slicing, it is necessary to amplify the pulses. However, the ASE from the amplifier can affect the spectrum. That is why another filter at the amplifier output must be used.
Reproducibility of measurements is very important. It is critically dependent on the stability of the laser. The spectrum must be measured at various places of the experimental setup (at the outputs from the laser, amplifiers, nonlinear fibre and filters). In our experiments, an optical switch was used in order to eliminate an uncertainty in insertion loss due to the need of repeated manipulation with the connectors.

References

[1] Blaze Photonics, Compact ultra-bright supercontinuum light source, http://www.blazephotonics.com/support/Supercontinuum%20-%20SC-5.0-1040.pdf.

[2] P.A. Andersen, "Supercontinuum generation in a Photonic Crystal fibre using picosecond pulses at 1550 nm," Transparent Optical Networks **1**, 66-69 (2003), http://ieeexplore.ieee.org/search/wrapper.jsp?arnumber=1264581.

[3] H.J.R. Dutton, Understanding Optical Communications, Prentice-Hall (1998), http://www.ar-ent.net/dar/arlib32/out/html/man/redbooks/sg245230.pdf.

[4] IMRA, Progress in femtosecond fibre lasers, www.imra.com/pdf/Tutorial1.pdf.

[5] B. E. A Saleh, M. C. Teich, *Základy fotoniky 1-4*, Matfyzpress, Praha 1994.

[6] C. Billet, J. Dudley, N. Joly, and J. Knight, "Intermediate asymptotic evolution and photonic bandgap fiber compression of optical similaritons around 1550 nm," Opt. Express **13**, 3236-3241 (2005), http://www.opticsinfobase.org/abstract.cfm?URI=oe-13-9-3236.

[7] Crystal Fibre, Nonlinear Photonic Crystal Fibre – NL-1550-NEG-1, http://www.crystal-fibre.com/datasheets/NL-1550-NEG-1.pdf.

[8] V. V. R. Kumar, A. George, W. Reeves, J. Knight, P. Russell, F. Omenetto, and A. Taylor, "Extruded soft glass photonic crystal fiber for ultrabroad supercontinuum generation," Opt. Express **10**, 1520-1525 (2002), http://www.opticsinfobase.org/abstract.cfm?URI=oe-10-25-1520.

[9] K. Saitoh and M. Koshiba, "Highly nonlinear dispersion-flattened photonic crystal fibers for supercontinuum generation in a telecommunication window," Opt. Express **12**, 2027-2032 (2004), http://www.opticsinfobase.org/abstract.cfm?URI=oe-12-10-2027.

[10] T. Yamamoto, H. Kubota, S. Kawanishi, M. Tanaka, and S. Yamaguchi, "Supercontinuum generation at 1.55 μm in a dispersion-flattened polarization-maintaining photonic crystal fiber," Opt. Express **11**, 1537-1540 (2003), http://www.opticsinfobase.org/abstract.cfm?URI=oe-11-13-1537.

[11] J. Gopinath, H. Shen, H. Sotobayashi, E. Ippen, T. Hasegawa, T. Nagashima, and N. Sugimoto, "Highly nonlinear bismuth-oxide fiber for smooth supercontinuum generation at 1.5 μm," Opt. Express **12**, 5697-5702 (2004), http://www.opticsinfobase.org/abstract.cfm?URI=oe-12-23-5697.

[12] G. Genty, M. Lehtonen, H. Ludvigsen, J. Broeng, and M. Kaivola, "Spectral broadening of femtosecond pulses into continuum radiation in microstructured fibers," Opt. Express **10**, 1083-1098 (2002), http://www.opticsinfobase.org/abstract.cfm?URI=oe-10-20-1083.

[13] Z. Zhu and T. Brown, "Effect of frequency chirping on supercontinuum generation in photonic crystal fibers," Opt. Express **12**, 689-694 (2004), http://www.opticsinfobase.org/abstract.cfm?URI=oe-12-4-689.

[14] H. Takara, Multiple Optical Carrier Generation, Optics and Photonics News, 48-51, March 2002, http://www.osa-opn.org/abstract.cfm?URI=OPN-13-3-48.

[15] P. Rakich, H. Sotobayashi, J. Gopinath, S. Johnson, J. Sickler, C. Wong, J. Joannopoulos, and E. Ippen, "Nano-scale photonic crystal microcavity characterization with an all-fiber based 1.2 – 2.0 μm supercontinuum," Opt. Express **13**, 821-825 (2005), http://www.opticsinfobase.org/abstract.cfm?URI=oe-13-3-821.

[16] A. Saliminia, S. L. Chin, and R. Vallée, "Ultra-broad and coherent white light generation in silica glass by focused femtosecond pulses at 1.5 um," Opt. Express **13**, 5731-5738 (2005), http://www.opticsinfobase.org/abstract.cfm?URI=oe-13-15-5731.

[17] C. Finot, G. Millot, C. Billet, and J. Dudley, "Experimental generation of parabolic pulses via Raman amplification in optical fiber," Opt. Express **11**, 1547-1552 (2003), http://www.opticsinfobase.org/abstract.cfm?URI=oe-11-13-1547.

[18] C. Finot and G. Millot, "Synthesis of optical pulses by use of similaritons," Opt. Express **12**, 5104-5109 (2004), http://www.opticsinfobase.org/abstract.cfm?URI=oe-12-21-5104.

[19] G. P. Agrawal, *Nonlinear Fibre Optics*, Academic Press, San Diego 1989.

[20] J. Kaňka, "Numerical simulation of subpicosecond soliton formation in a nonlinear coupler laser," Optics Letters, Vol. **19**, No. 22, November 1994.

[21] P. D. Drummond and J. F. Corney, "Quantum noise in optical fibers. I. Stochastic equations ," J. Opt. Soc. Am. B 18, 139-152 (2001), http://www.opticsinfobase.org/abstract.cfm?URI=josab-18-2-139.

[22] J. F. Corney and P. D. Drummond, "Quantum noise in optical fibers. II. Raman jitter in soliton communications ," J. Opt. Soc. Am. B **18**, 153-161 (2001), http://www.opticsinfobase.org/abstract.cfm?URI=josab-18-2-153.

[23] L. E. Nelson, D. J. Jones, K. Tamura, H. A. Haus, and E. P. Ippen, "Ultrashort-pulse fiber ring lasers," Appl. Phys. B 65, 277-294 (1997).

[24] F. Ö. İlday et al., *Self-similarly Evolving Pulses for High-Energy Fiber Lasers*, Optics and Quantum Electronics Group, MIT, Cambridge, MA, 2003.

[25] Gatech, Intensity Autocorrelation, http://www.physics.gatech.edu/gcuo/Tutorial/AC.pdf.

[26] X. Liu, B. Lee, "A Fast method for nonlinear Schödinger equation," IEEE Photonics Technology Letters, Vol. **15**, No. 11, November 2003.

Appendix A - Numerical method for solving the propagation equation

From the mathematical point of view, the propagation equation (4.2.28) is a nonlinear partial integro-differential equation, which has not analytic solution, except for some specific cases. Therefore, numerical methods are used. One method that is used extensively [19] is a pseudospectral method called the symmetrized split-step Fourier method (S-SSFM).

To show the principle the S-SSFM, let us write the propagation equation formally in the form

$$\frac{\partial A}{\partial z} = (\hat{D} + \hat{N})A, \tag{A.1}$$

where $\hat{D}$ is a linear differential operator which includes dispersive, gain and absorption effects and $\hat{N}$ is a nonlinear operator which includes the nonlinear effects. These operators for (4.2.28) can be expressed by

$$\hat{D} = -\frac{i}{2}\beta_2\frac{\partial^2}{\partial T^2} + \frac{1}{6}\beta_3\frac{\partial^3}{\partial T^3} - \frac{\alpha}{2}, \tag{A.2}$$

$$\hat{N} = i(1-f_R)\gamma|A|^2 + i\gamma f_R\int_{-\infty}^{T} h_R(T-T')|A(z,T')|^2\,dT'. \tag{A.3}$$

The fibre length is divided into many short sections of length h, where dispersive and nonlinear effects are assumed to act independently. On the distance from z to $z + h/2$, the pulse is propagating only with dispersion. At $z + h/2$, the influence of the nonlinear operator over the whole section length h is included. After that, the pulse is propagating distance from $z + h/2$ to $z + h$ only with dispersion. This procedure can be expressed by the relation

$$A(z+h,T) \simeq \exp\left(\frac{h}{2}\hat{D}\right)\exp\left(\int_z^{z+h}\hat{N}(z')dz'\right)\exp\left(\frac{h}{2}\hat{D}\right)A(z,t). \tag{A.4}$$

The operator $\exp\left(\frac{h}{2}\hat{D}\right)$ is evaluated in the Fourier domain, where the differential operator $\partial/\partial T$ is replaced by $i\omega$, what is only a number in the Fourier domain. Thus, the prescription of execution of $\exp\left(\frac{h}{2}\hat{D}\right)$ is

$$\exp\left(\frac{h}{2}\hat{D}\right)A(z,T) = \left\{F^{-1}\exp\left[\frac{h}{2}\hat{D}(i\omega)\right]F\right\}A(z,T), \tag{A.5}$$

where F stands for the Fourier transform.

The simplest way how to evaluate the integral $\int_z^{z+h}\hat{N}(z')dz'$ is to make approximation

$$\int_{z}^{z+h} \hat{N}(z')dz' \simeq h\hat{N}(z). \tag{A.6}$$

This approximation can be used for the small step size h. More accurately, the integral can be evaluated by the trapezoidal rule to obtain

$$\int_{z}^{z+h} \hat{N}(z')dz' \simeq \frac{h}{2}\left[\hat{N}(z)+\hat{N}(z+h)\right], \tag{A.7}$$

where $\hat{N}(z+h)$ must be evaluated by the iterative method. $\hat{N}(z+h)$ is initially replaced by $\hat{N}(z)$ to estimate the value $A(z+h,T)$, which is then used to calculate $\hat{N}(z+h)$ again. Performance of S-SSFM was further improved, for example by introducing the predictor-corrector method [26].